Near Shannon Limit and Reduced Peak to Average Power Ratio Channel Coded OFDM

Thesis advisor

Vahid Tarokh

Author

Yongjun Kwak

Near Shannon Limit and Reduced Peak to Average Power Ratio Channel Coded OFDM

Abstract

Solutions to the problem of large peak to average power ratio (PAPR) in orthogonal frequency division multiplexing (OFDM) systems are proposed. Although the design of PAPR reduction codewords has been extensively studied and the existence of asymptotically good codes with low PAPR has been proved, still no reduced PAPR capacity achieving code has been constructed. This is the topic of the current thesis.

This goal is achieved by implementing a time-frequency turbo block coded OFDM. In this scheme, we design the frequency domain component code to have a PAPR bounded by a small number. The time domain component code is designed to obtain good performance while the decoding algorithm has reasonable complexity. Through comparative numerical evaluation we show that our method achieves considerable improvement in terms of PAPR with slight performance degradation compared to capacity achieving codes with similar block lengths. For the frequency domain component code, we used the realization of Golay sequences as cosets of the first order Reed-Muller code and the modification of dual BCH code. A simple MAP decoding algorithm for the modified dual BCH code is also provided.

Finally, we provide a flexible and practical scheme based on probabilistic approach

to a PAPR problem. This approach decreases the PAPR without any significant performance loss and without any adverse impact or required change to the system.

Contents

List of Figures

List of Tables

Acknowledgments

Foremost, I would like to express my sincere gratitude to my advisor, Prof. Vahid Tarokh for all his support, patience, and engouragement. He has guided me greatly in all the time of research and writing of this thesis. I could not have imagined having a better advisor for my Ph.D study.

I would like to thank Prof. Reza Nezafat, my research supervisor at Beth Israel Deaconess Medical Center for all his support, advice, and guidance . He gave me a great opportunity to work on the new field, MR imaging during the later part of my Ph.D program.

I would like to thank the rest of my thesis committee: Prof. Roger Brockett and Prof. Yue Lu, for their insightful comments and questions for this thesis.

I would like to thank Prof. Besma Smida for her help on my research. She is a great coordinator, a nice collaborator, and a good friend.

I was pretty happy working with nice people in Vahid's group and Reza's group. It was really good to work with them and to have such good friends.

I would like to thank my family with all my heart. Throughout my Ph.D program, my wife, Jiyeon Park has provided me with great support, encouragement, and endless love. I thank her for following me here, being so patient, giving such great support, and most importantly giving me Jaemin and Jaehoon, the loveliest two sons.

Finally, I would like to thank my father, Minhwan Kwak and my late mother, Chaehee Cho for giving birth to me, supporting me throughout my life, and giving me the chance to write this thesis.

Dedicated to Jiyeon, Jaemin, Jaehoon,
my father,
and my late mother.

Chapter 1

Introduction

Orthogonal Frequency Division Multiplexing (OFDM) is a promising data multiplexing technique for the wireless communication. It provides high spectral efficiency and simple modulation and demodulation algorithms. Furthermore, OFDM reduces the requirement for equalization and enhances the system capacity by adapting to the channel conditions in the frequency domain. In spite of these advantages, OFDM is not widely used in the reverse link of the modern mobile communication systems because of its high Peak to Average Power Ratio (PAPR). Typically, significant portion of the total cost of OFDM base stations corresponds to that of power amplifiers. This is due to the fact that comparatively large linear region is required for the power amplifiers in OFDM systems. In general, an engineering rule of thumb is that for every 3 dB increase in the linear region of power amplifiers, the cost of the power amplifier doubles. OFDM transmission requires a large power amplifier linear region because of its relatively high PAPR. Thus OFDM power amplifiers may have more stringent requirements, which can be an issue in OFDM system design.

In addition to the cost, the high PAPR of OFDM signals has other adverse effects. For instance, if the peak transmit power is restricted due to regulatory or design constraints, the large PAPR of the OFDM signals forces reduction in the mean power of the signal, effectively reducing the range of the transmission and the transmit power efficiency. This is the main barrier to the adaptation of OFDM system in the reverse link of the mobile system.

In this light, the design of the OFDM system with high performance capacity and reduced PAPR remains extremely important, albeit a very difficult problem to solve. In this thesis, we propose an elegant approach to produce a solution for this problem. The contributions of this thesis are three methods for achieving reduced PAPR. The new channel coding structure, time-frequency turbo block code is proposed as a general platform of utilizing PAPR reduction codewords. For achieving reduced PAPR, Golay sequences that were proven to have bounded PAPR are applied to the time-frequency turbo block code. The Golay sequences can be realized by cosets of the first order Reed-Muller code. Furthermore, by having the reduced PAPR property of dual BCH code and providing a simple MAP decoding algorithm of the augmented code of the dual BCH, we utilize this code as an alternative candidate for the time-frequency turbo block code. And finally, a probabilistic approach is provided as another way of reducing PAPR without any modification of the existing channel coding structure.

1.1 Structure of This Thesis

The rest of the thesis is divided into five chapters:

- Chapter 2 gives brief overview to fundamentals of Orthogonal Frequency Divi-

sion Multiplexing (OFDM). We discuss some basic OFDM signal representation, pros and cons of OFDM, and modulation and demodulation schemes. We will also discuss the Peak to Average Power Ratio (PAPR) problem.

- Chapter 3 proposes the new Turbo Block Code (TBC) structure that achieves reduced PAPR and near capacity performance for some parameters and rates of interest. The frequency domain signals are based on the realization of Golay sequences of cosets of Reed-Muller code. The coding rates may be low, so we also provide an enhancement these systems with higher transmission rates.

- Chapter 4 provides a modification of dual BCH codes amenable to a simple MAP decoding algorithm. We will then apply the proposed modification in TBC structure to have reduced PAPR and near capacity performance.

- In Chapter 5, we consider the probabilistic approach to PAPR reduction using channel coding. We proposed a simple PAPR reduction scheme which can be utilized with any channel coding method amenable to soft-in/soft-out decoding. Proposed scheme provides significant PAPR reduction with negligible performance loss and no adverse system impact.

- Finally, we summarize contributions of this thesis in Chapter 6.

Chapter 2

Principles of OFDM

This chapter briefly introduces the basic Principles of Orthogonal Frequency Division Multiplexing (OFDM).

2.1 Introduction

The principle of Orthogonal Frequency Division Multiplexing (OFDM) is to split a high-rate data stream into a number of lower rate streams that are transmitted simultaneously over a number of orthogonal subcarriers. Followings are summary of advantages and drawbacks of OFDM transmission.

Key advantages of OFDM transmission scheme

- By allowing frequency overlap, we can achieve high spectral efficiency.
- OFDM is an efficient way to deal with multi-path; the implementation complexity is significantly lower than that of a single carrier system.

- In frequency selective channels, it is possible to enhance the capacity by adapting the data rate per subcarrier or a set of subcarriers according to the signal-to-noise ratio of the particular subcarriers.

- It is computationally efficient by using FFT techniques to implement the modulation and demodulation functions

Drawbacks of OFDM transmission scheme

- OFDM is sensitive to frequency offset and phase noise

- OFDM has a relatively large peak-to-average power ratio, which tends to reduce the power efficiency of the RF amplifier and increase the cost of the transmitter. More details would be provided in Section 2.3.

In a classical parallel data system, the total single frequency band is divided into N non-overlapping frequency subchannels and data are multiplexed using Frequency Division Multiplexing (FDM) as shown in Figure 2.1 (a). FDM method is good to eliminate interchannel interference, but this leads to inefficient use of frequency resources. To improve the efficiency, it was proposed to use parallel data and FDM with overlapping subchannels as shown in Figure 2.1 (b). To realize the overlapping multicarrier technique, we need to have orthogonality between the different modulated carriers (subcarriers). Section 2.2 discusses the achievements of orthogonality between subcarriers in detail.

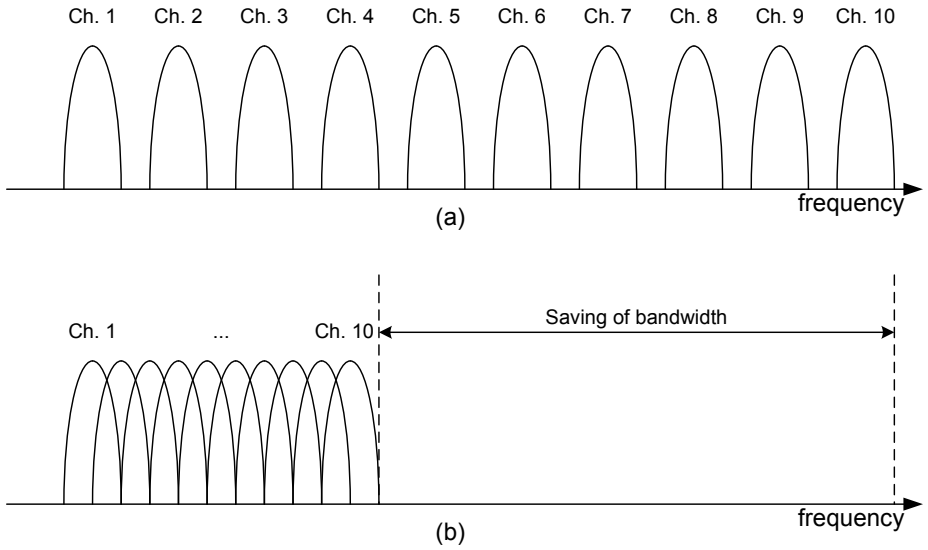

Figure 2.1: Concept of OFDM signal: (a) Conventional multicarrier technique (FDM), and (b) orthogonal multicarrier modulation technique (OFDM)

2.2 OFDM Transmission and Reception

The contents of this section is based on [1].

2.2.1 OFDM Modulation

As stated in Section 2.1, OFDM transmits data using multiple subcarriers. The followings are fundamental characteristics of OFDM transmission.

- The use of large number of narrowband subcarriers.
- Multiple subcarriers with a very short subcarrier spacing $\Delta f = 1/T_u$, where T_u is the modulation-symbol time and Δf is the subcarrier spacing (see Figure 2.2).

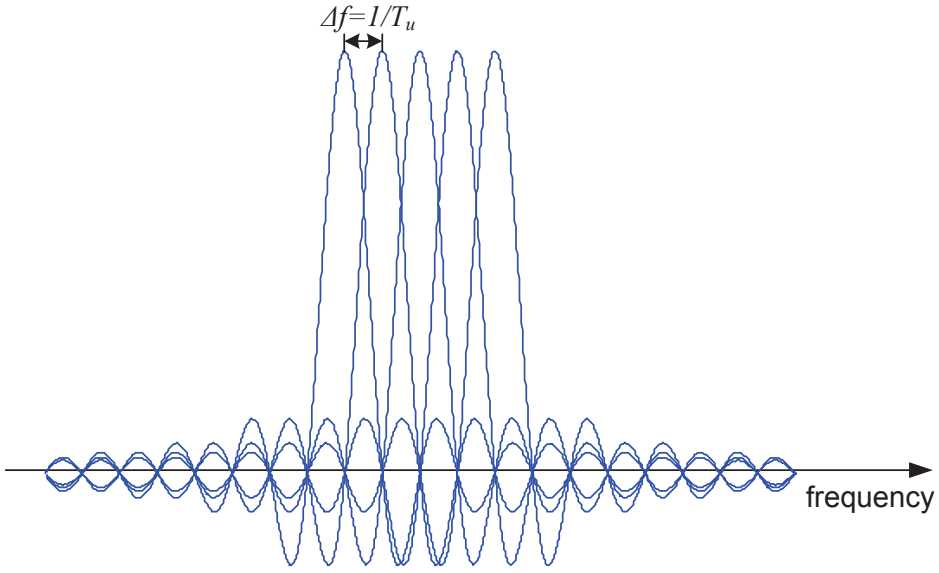

Figure 2.2: OFDM subcarrier spacing.

A basic OFDM modulator is illustrated in Figure 2.3. It consists of N_c complex modulators, where each modulator corresponds to one OFDM subcarrier. A basic OFDM signal $S_{\boldsymbol{c}}(t)$ during the time interval $mT_u \leq t < (m+1)T_u$ can thus be expressed as

$$\begin{aligned} S_{\boldsymbol{c}}(t) &= \sum_{k=0}^{N-1} S_{\boldsymbol{c}}^{(k)}(t) \\ &= \sum_{k=0}^{N-1} c_k^{(m)} \exp(j2\pi f_k t) \end{aligned} \tag{2.1}$$

where $S_{\boldsymbol{c}}^{(k)}(t)$ is the k–th modulated subcarrier with frequency $f_k = f_0 + k\Delta f$, where f_0 is the beginning frequency, and $c_k^{(m)}$ is the modulation symbol applied to the k–th subcarrier during the m–th OFDM symbol interval. During each OFDM symbol interval, N OFDM-modulated symbols are transmitted in parallel using N subcarriers. The modulation symbols can be from any modulation alphabet, such as

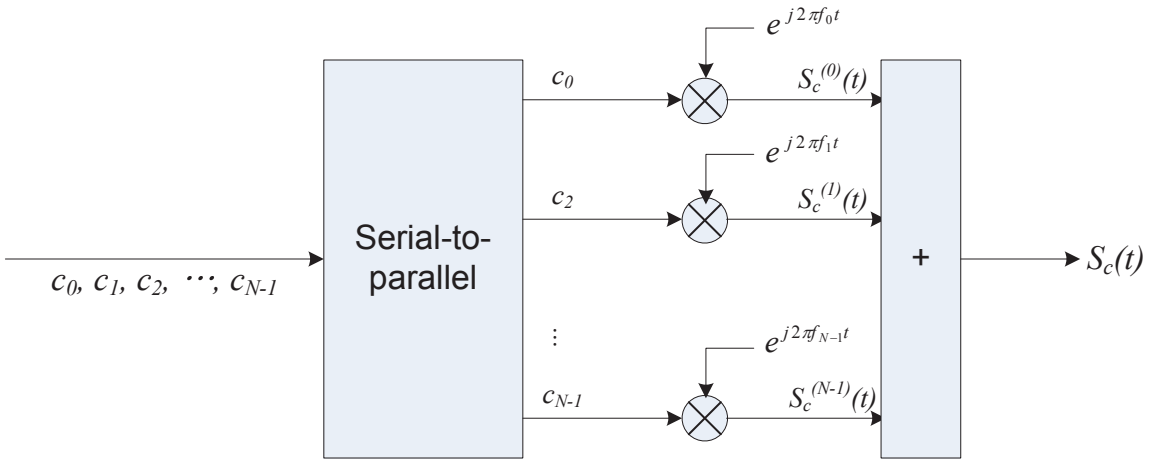

Figure 2.3: OFDM modulation.

QPSK, 16–QAM, or 64–QAM.

The term Orthogonal in OFDM is based on the fact that two modulated OFDM subcarriers are mutually orthogonal over OFDM symbol interval, $mT_u \leq t < (m+1)T_u$. It can be expressed as the Equation (2.2).

$$\begin{aligned}\int_{mT_u}^{(m+1)T_u} S_{\mathbf{c}}^{(k_1)}(t) S_{\mathbf{c}}^{(k_2)^*}(t) &= \int_{mT_u}^{(m+1)T_u} c_{k_1} c_{k_2} e^{j2\pi(f_0+k_1\Delta f)t} e^{-j2\pi(f_0+k_2\Delta f)t} dt \\ &= \int_{mT_u}^{(m+1)T_u} c_{k_1} c_{k_2} e^{j2\pi(k_1-k_2)\Delta f t} dt \\ &= \begin{cases} c_{k_1}^2 T_u & k_1 = k_2 \\ 0 & k_1 \neq k_2 \end{cases}\end{aligned} \tag{2.2}$$

The physical resource for the OFDM transmission is often defined as a 2-dimensional time-frequency block as seen in Figure 2.4 where each column of a block corresponds to one OFDM symbol and each row of a block corresponds to one OFDM subcarrier.

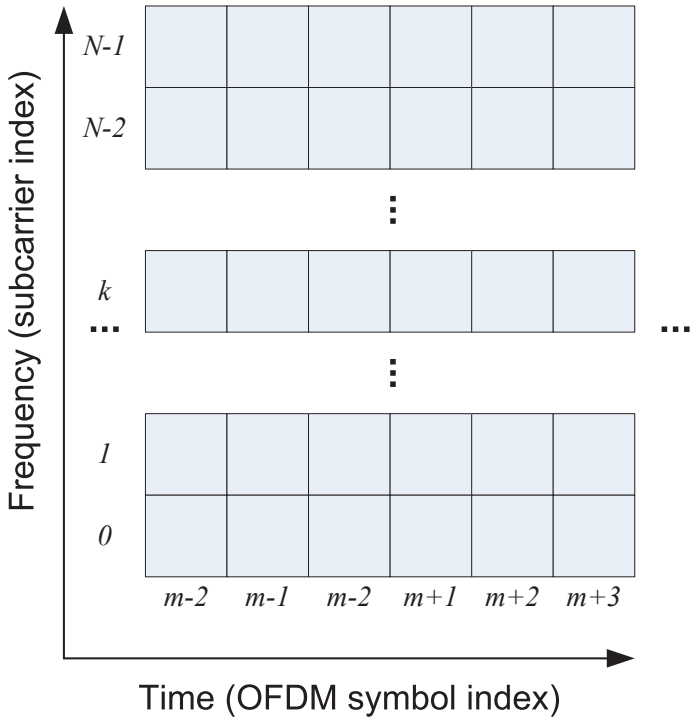

Figure 2.4: OFDM time-frequency resource.

2.2.2 OFDM Demodulation

The basic principle of OFDM demodulation consists of a block of correlators as seen in Figure 2.5. It is the most important for the demodulator that orthogonality should be guaranteed between subcarriers. In other words, one OFDM subcarriers do not cause any interference to any other subcarriers after demodulation. Thus the avoidance of interference between OFDM subcarriers is not simply due to a subcarrier spectrum separation, but rather the subcarrier orthogonality is due to the specific frequency-domain structure of each subcarrier in combination with the specific choice of a subcarrier spacing Δf equal to the per-subcarrier symbol rate $1/T_u$.

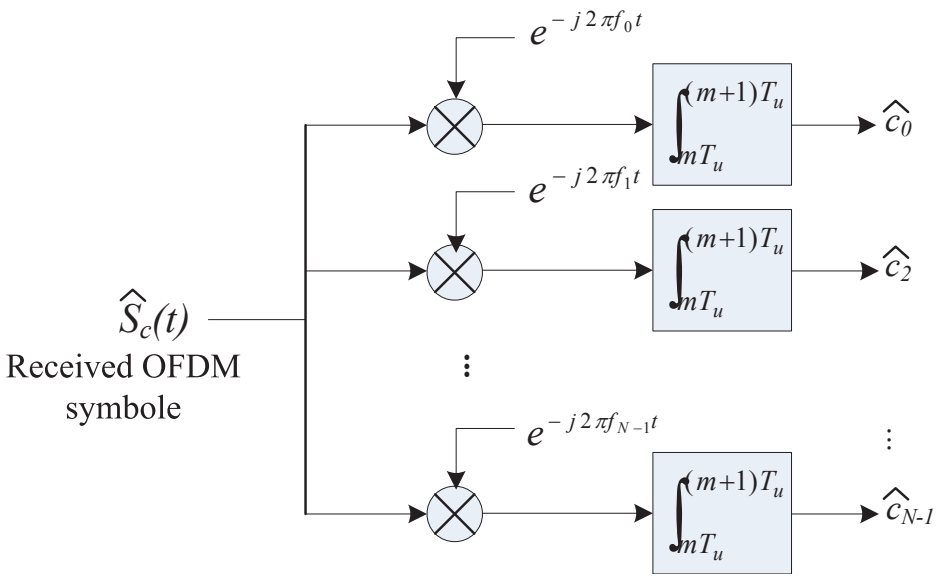

Figure 2.5: OFDM demodulation.

2.2.3 OFDM and Fourier Transform

Figure 2.3 and Figure 2.5 are illustrating the basic OFDM modulation and demodulation schemes. However, these are not the most efficient modulator/demodulator structures considering implementation complexity. Considering the inverse relationship between subcarrier spacing and OFDM symbol duration, the complex OFDM signal as defined by Equation (2.1) is in fact nothing more than the inverse Fourier transform of N input symbols.

Let's consider a discrete time OFDM signal where the sampling rate f_s is equal to $N\Delta f$. In this case, we know that $\Delta f T_s = \frac{1}{N}$, where T_s is the sampling period such that $T_s = 1/f_s$. With these assumptions, the time-discrete OFDM signal can be expressed as:

$$\begin{aligned} s_n &= S_{\boldsymbol{c}}(nT_s) \\ &= \sum_{k=0}^{N-1} c_k e^{j2\pi k\Delta f n T_s} \\ &= \sum_{k=0}^{N-1} c_k e^{j2\pi kn/N} \end{aligned} \tag{2.3}$$

Thus, the sampled OFDM signal x_n is the size-N Inverse Discrete Fourier Transform (IDFT) of the modulation symbols $c_0, c_1, \cdots, c_{N-1}$. Normally, IDFT is implemented by the complexity efficient Inverse Fast Fourier Transform (IFFT) processing. Similar to OFDM modulation, efficient FFT processing can be used for OFDM demodulation, replacing N demodulators of Figure 2.5.

2.3 PAPR Problem in OFDM Systems

The OFDM signal at time t is modeled as given in Equation (2.1)

$$S_{\boldsymbol{c}}(t) = \sum_{k=0}^{N-1} c_k e^{j2\pi f_k t} \tag{2.4}$$

For any sequence c_k, the instantaneous power of the corresponding transmitted signal $\Re(S_{\boldsymbol{c}}(t))$ is equal to $\Re(S_{\boldsymbol{c}}(t))^2$. This power is less than or equal to the function $|S_{\boldsymbol{c}}(t)|^2$, called the *envelope power* of the OFDM signal. The *peak-to-average power ratio* (PAPR) of the OFDM signal, is defined to be the ratio of the peak power of $\Re(S_{\boldsymbol{c}}(t))$ to $\|\boldsymbol{c}\|^2$, the average envelope power.

$$\mathrm{PAPR}(\boldsymbol{c}) = \max_{0\le t\le 1} \frac{\left|\Re(S_{\boldsymbol{c}}(t))\right|^2}{\|\boldsymbol{c}\|^2} \tag{2.5}$$

The complex modulation symbol c_k is assigned to the k–th subcarrier of an OFDM system during a given symbol period. We simply assume that the sequence $\mathbf{c} =$

$(c_0, c_1, \cdots, c_{N-1})$ is modulated from the $\mathbb{Z}_H$–ary sequence $\boldsymbol{a} = (a_0, a_1, \cdots, a_{N-1})$, i.e. $\mathbf{c} = (c_0, c_1, \cdots, c_{N-1}) = (\xi^{a_0}, \xi^{a_1}, \cdots, \xi^{a_{N-1}})$, where $\xi = \exp(2\pi j/H)$ is a primitive H–th root of unity. This modulation is called H–phase shift keying, which in the cases $H = 2$ or 4 is also known as binary phase–shift keying (BPSK) or quadrature phase–shift keying (QPSK), respectively.

Then the OFDM signal can be written as

$$\begin{aligned} S_{\boldsymbol{c}}(t) &= \sum_{k=0}^{N-1} \xi^{a_k} \exp(2\pi j(f_0 + kf_s)t) \\ &= \sum_{k=0}^{N-1} \xi^{a_k + Hf_k t} \end{aligned} \tag{2.6}$$

where f_k is the frequency of the k–th sub-carrier. We guarantee the orthogonality between subcarriers by having

$$f_k = f_0 + k\Delta f \tag{2.7}$$

The instantaneous envelope power of the signal is the real-valued function $P(t) = |S_{\boldsymbol{c}}(t)|^2$, and substitution from Equation (2.6) and Equation (2.7) gives,

$$\begin{aligned} P(t) &= |S_{\boldsymbol{c}}(t)|^2 \\ &= S_{\boldsymbol{c}}(t) \cdot S_{\boldsymbol{c}}(t)^* \\ &= \sum_{k=0}^{N-1} \xi^{a_k + Hf_k t} \cdot \sum_{i=0}^{N-1} \xi^{-(a_i + Hf_i t)} \\ &= \sum_{k=0}^{N-1} \sum_{i=0}^{N-1} \xi^{a_k - a_i + H(k-i)\Delta f t}. \end{aligned} \tag{2.8}$$

Then by putting $i = k + u$ in the expression for $P_a(t)$ given by Equation (2.8) we

obtain

$$\begin{aligned} P(t) &= N + \sum_{u\neq 0}\sum_{k} \xi^{a_k - a_{k+u} - Hu\Delta ft} \\ &= N + \sum_{u\neq 0} C(u)\xi^{-Hu\Delta ft} \end{aligned} \tag{2.9}$$

where $C(u) = \sum_k \xi^{a_k - a_{k+u}}$.

The *peak envelope power* (PEP) of the sequence $\boldsymbol{a}$ is the supremum over a symbol period of $P(t)$. From Equation (2.9), the mean envelope power of any sequence $\boldsymbol{a}$ over a symbol period is n, and so the *peak-to-mean envelope power ratio* (PMEPR) of $\boldsymbol{a}$ is the ratio PEP$/N$. From Equation (2.9) we see that

$$P(t) \leq N + \sum_{u\neq 0} |C(u)| \cdot 1 \leq N + 2\sum_{u=1}^{N-1}(N-u) = N^2 \tag{2.10}$$

So the PEP of any sequence $\boldsymbol{a}$ is at most N^2. Therefore, the relationship between PAPR and PMEPR is shown as:

$$\mathrm{PAPR}(\boldsymbol{c}) = \max_{0\leq t\leq 1} \frac{|\Re(S_{\boldsymbol{c}}(t))|^2}{\|\boldsymbol{c}\|^2} \leq \frac{\max P(t)}{\|\boldsymbol{c}\|^2} = PMEPR(\leq \frac{N^2}{N} = N). \tag{2.11}$$

In conclusion, the PAPR of an OFDM symbols having $\mathbb{Z}_H$–ary modulated symbol sequences $\mathbf{c} = (c_0, c_1, \cdots, c_{N-1})$ is at most N, which is very high compared to single carrier modulations methods.

To satisfy the spectral masks imposed by regulatory agencies and to overcome the implementation constraints in the nonlinear amplifier design, investigating methods to generate a signal with favorable PAPR properties is of vital importance. With high PAPR values, amplifiers having large power back-off values are required. If the amplifier back-off is not adequate, then the nonlinear characteristics of the amplifier distorts the in-band signal and creates the out-of-band interference with adjacent

channels [2]. However, increasing the back-off of the amplifier, not only reduces the power efficiency but also rises the amplifier cost significantly. Several PAPR reduction schemes have been extensively studied for multi-carrier systems. A category of these techniques, including selected mapping and partial transmit signaling, reduces the probability of generating a signal with large PAPR while it necessitates the transmission of side information [3, 4]. There are also PAPR reduction methods, such as clipping, which do not require transmission of side information, at the expense of other adverse effects such as spectral regrowth [5]. An interesting approach is to deal with the problem in the framework of channel coding. This approach, was first proposed in [6] in which the codewords with low PAPR are determined by an exhaustive search. There have been other PAPR reducing techniques which is utilizing coding techniques for improving the bit error rate [7, 8, 9]. Despite extensive research on PAPR reduction algorithms, none of the proposed methods based on channel coding have been utilized in practice. The main reason is the loss in spectral efficiency as OFDM block length increases and the poor error correcting capability of the proposed schemes. Therefore, the design of a capacity achieving code for which all codewords generate low PAPR OFDM signals, is still an important open problem.

2.4 Summary

Chapter 2 introduces basic principles of OFDM system including transmission and reception schemes. And this also discusses about the serious PAPR problem of OFDM system. Therefore, the main motivation of this thesis is to develop the channel coding structures that resolve the PAPR problem.

Chapter 3

Time-Frequency Turbo Block Coded OFDM

3.1 Introduction

As we discussed in Section 2.3, high fluctuations in the signal amplitude of multi-carrier systems such as OFDM system, generated by the constructive addition of a large number of sub-carriers, is considered as the principal drawback of these systems, known as PAPR problem [10]. Various methods have been proposed to solve this PAPR problem. As discussed in Section 2.3, an interesting category for the PAPR-alleviating approach is to use the channel coding method to generate codewords of reduced PAPR. This approach was first proposed in [6]. Although the method of [6] provides a worst case guarantee for PAPR, it entails an exhaustive search which increases the computational complexity specially for large number of subcarriers. Furthermore since in this solution the encoding and decoding are also performed by

the use of look-up tables, it also requires large memory when the OFDM block length increases. In [11], the selection of the appropriate codeword is developed based on specific sequences such as Shapiro-Rudin and Golay sequences. However, neither in [6] nor in [11] the error correcting issue has been addressed. The study in [7] discusses the error correction problem where first a powerful block code is selected and then by using a weight vector the PAPR of the codeword is decreased. The theoretical aspects of the relation between the code rate, minimum Euclidean distance of the code and its block length is provided in [12] as two fundamental theorems. The first theorem proves a lower bound for PAPR based on the three aforementioned parameters. The second theorem provides a lower bound for the code rate as a function of maximum acceptable PAPR, code block length and code minimum distance. Despite all the research on this subject, the error correction capability of coding-based PAPR reduction methods has not been paid the attention it deserves. Through the effort of seeking a relationship between PAPR and error correction probability, [13] showed that finding the PAPR of a code is associated with minimum distance decoding of the code. Moreover, a sophisticated algorithm is presented in [13] to find the weight vector discussed in [7]. In [14], a new class of Reed-Muller code with reduced PAPR is proposed. Although the error correction properties of RM code has been well-studied, the performance of this code is quite far from the Shannon limit and can not compete with that of the capacity achieving codes, e.g. turbo codes [15] or LDPC codes [16]. Therefore the problem of designing codes that perform close to the Shannon limit while having good PAPR properties has remained unsolved.

In this chapter, a time-frequency turbo block code (TBC) is proposed to solve the

problem of achieving good BER performance with a reduced PAPR. The frequency domain component code is designed such that it provides codewords with low PAPR. For the choice of time domain code, the code with good error correction performance is an appropriate candidate to compensate the comparatively low error correction capability of RM code. The decoding of TBC is accomplished in an iterative manner using soft-in/soft-out decoders of each component code. I exhibit the superiority of this scheme by examining the performance and amplitude distribution of other codes with similar code rates.

3.2 PAPR and Reed-Muller Code

3.2.1 Golay Sequences

The upper bound of n for PMEPR is attained by the sequence $\boldsymbol{a} = (0, 0, \cdots, 0)$ of length n, which can occur in an uncoded OFDM system. But by restricting the set of allowed sequences to Golay sequences we can reduce the PMEPR from its maximum value of n to at most 2. The definition of the Golay sequence is given below.

Definition 3.2.1 *Let*

$$\boldsymbol{a} = (a_0, a_1, \cdots, a_{n-1})$$

and

$$\boldsymbol{b} = (b_0, b_1, \cdots, b_{n-1})$$

where $a_i, b_i \in \mathbb{Z}_H$. *The sequences* $\boldsymbol{a}$ *and* $\boldsymbol{b}$ *are called a Golay complementary pair over* $\mathbb{Z}_H$ *of length* n *if* $C_a(u)+C_b(u) = 0$ *for each* $u \neq 0$, *where* $C_a(u) = \sum_k e^{(2\pi j/H)(a_k - a_{k+u})}$.

Any sequence which is a member of a Golay complementary pair is called Golay sequence,

Golay complementary pairs were introduced by Golay [17, 18]. The upper bound of the PMEPR of Golay sequence is given in Theorem 3.2.1, which was proved in [19].

Theorem 3.2.1 *The PMEPR of any Golay sequence is at most 2.*

The proof of Theorem 3.2.1 is simple. Let $\boldsymbol{a}$ and $\boldsymbol{b}$ be a Golay complementary pair of length N, so that by definition $C_a(u)+C_b(u) = 0$ for each $u \neq 0$. Then from Equation (2.9), $P_a(t) + P_b(t) = 2N$ and since $P_b(t) = |S_b(t)|^2 \geq 0$, we deduce $P_a(t) \leq 2N$. $\text{PMEPR}(\boldsymbol{a}) = \frac{\max P_a(t)}{\|\boldsymbol{a}\|^2} \leq \frac{2N}{N} = 2$. □

Theorem 3.2.2 and Corollary 3.2.1, proved in [14], are explaining how to generate Golay sequences using monomials in the boolean functions.

Definition 3.2.2 *A Boolean function is a function f from*

$$\mathbb{Z}_2^m = \{(x_1, x_2, \cdots, x_m) | x_i \in \{0, 1\}\} \tag{3.1}$$

to $\mathbb{Z}_2$. We regard each 0–1 variable x_i as itself being a Boolean function $f_i(x_1, x_2, \cdots, x_m) = x_i$ and consider the 2^m monomials

$$1, x_1, x_2, \cdots, x_m, x_1x_2, x_1x_3, \cdots, x_{m-1}x_m, \cdots, x_1x_2\cdots x_m. \tag{3.2}$$

We specify a sequence $\boldsymbol{f}$ of length 2^m corresponding to f by listing the values taken by $f(x_1, x_2, \cdots, x_m)$ as $(x_1, x_2, \cdots, x_m)$ ranges over all its 2^m values in lexicographic order. For example, for $m = 3$ we have

$$\boldsymbol{f} = (f(0,0,0), f(0,0,1), f(0,1,0), f(0,1,1), f(1,0,0), f(1,0,1), f(1,1,0), f(1,1,1))$$

and so we have these vectors $\mathbf{1} = (11111111)$, $\boldsymbol{x_1} = (00001111)$, $\boldsymbol{x_2} = (00110011)$, $\boldsymbol{x_3} = (01010101)$, $\boldsymbol{x_1x_2} = (00000011)$, and $\boldsymbol{x_2x_3} = (00010001)$.

Theorem 3.2.2 *Let*

$$f(x_1, x_2, \cdots, x_m) = 2^{h-1} \sum_{k=1}^{m-1} x_{\pi(k)} x_{\pi(k+1)} + \sum_{k=1}^{m} c_k x_k \tag{3.3}$$

where π is a permutation of the symbols $1, 2, \cdots, m$ and $c_k \in \mathbb{Z}_{2^h}$. Then the sequences

$$a(x_1, x_2, \cdots, x_m) = f(x_1, x_2, \cdots, x_m) + c$$

and

$$b(x_1, x_2, \cdots, x_m) = f(x_1, x_2, \cdots, x_m) + 2^{h-1} x_{\pi(1)} + c'$$

are a Golay complementary pair over $\mathbb{Z}_{2^h}$ of length 2^m for any $c, c' \in \mathbb{Z}_{2^h}$.

Corollary 3.2.1 *For any permutation π of the symbols $\{1, 2, \cdots, m\}$ and for any $c, c_k \in \mathbb{Z}_{2^h}$*

$$a(x_1, x_2, \cdots, x_m) = 2^{h-1} \sum_{k=1}^{m-1} x_{\pi(k)} x_{\pi(k+1)} + \sum_{k=1}^{m} c_k x_k + c \tag{3.4}$$

is a Golay sequence over $\mathbb{Z}_{2^h}$ of length 2^m.

3.2.2 Reed-Muller Codes

Binary Reed-Muller codes first appeared in print in 1954 and remain "one of the oldest and best understood families of codes" [20]. They have good error correction properties, provided the block length is not too large, and have the important practical advantage of being easy to decode. The r–th order binary Reed-Muller of length 2^m is defined as below [20].

Definition 3.2.3 *The r–th order binary Reed-Muller code RM(r,m) of length* $n = 2^m$*, for* $0 \geq r \geq m$*, is the set of all vectors* $\boldsymbol{f}$*, where* $f(x_1, x_2, \cdots, x_m)$ *is a Boolean function which is a polynomial of degree at most* r*.*

For example, codewords of the first order RM code of length 8 generated by

$$a_0\mathbf{1} + a_1\boldsymbol{x_1} + a_2\boldsymbol{x_2} + a_3\boldsymbol{x_3}, \quad a_i = 0 \text{ or } 1.$$

By combining Corollary 3.2.1 and Definition 3.2.3, we can simply get Corollary 3.2.2, as given in [14]:

Corollary 3.2.2 *Each of the* $m!/2$ *cosets of RM(*$1, m$*) in RM(*$2, m$*) having a coset representative of the form*

$$\sum_{k=1}^{m-1} x_{\pi(k)} x_{\pi(k+1)} \tag{3.5}$$

comprises 2^{m+1} *binary Golay sequences of length* 2^m*, where* π *is a permutation of the symbols* $(1, 2, \cdots, m)$

From Corollary 3.2.2, each of $\frac{m!}{2}$ cosets of RM$(1, m)$ in RM$(2, m)$ having a coset representative of the form $\sum_{k=1}^{m-1} x_{\pi(k)} x_{\pi(k+1)}$ comprises 2^{m+1} binary Golay sequences of length 2^m. Thus we conclude that for binary Reed-Muller codes, the PAPR of the codewords in the cosets does not exceed 3 dB [14].

We have seen that the PAPR of certain cosets of Reed-Muller code can be upper-bounded by 3dB. Then, we may have one question here: Can we use this Reed-Muller code for a practical OFDM system? Reed-Muller code may not be the best choice for the channel coding for the following reasons. First, even though Reed-Muller code has large minimum distance, its performance is relatively far from the optimum

performance, e.g. Shannon limit. Second, if we increase the code length, the rate of it decreases dramatically. Therefore we try to find an alternative coding structure which can keep the low-PAPR property of Reed-Muller code: turbo block code. Section 3.3 touches the Time-frequency turbo block code.

3.3 Low PAPR Turbo Block Code

3.3.1 Turbo Block Code: Encoding

Turbo block codes, also known as product codes, were first introduced in [21] and then developed in [22]. As opposed to the traditional turbo codes which are generated by concatenation of convolutional codes, TBC consists of two linear block codes. Let us consider two systematic linear block codes $\mathcal{C}^1$ with parameters (n_1, k_1, δ_1) and $\mathcal{C}^2$ with parameters (n_2, k_2, δ_2), where n_i, k_i and $\delta_i (i = \{1, 2\})$ stand for codeword length, number of information bits, and minimum Hamming distance, respectively. The product code $\mathcal{P} = \mathcal{C}^1 \otimes \mathcal{C}^2$is obtained (see Figure 3.1) by

1. placing $(k_1 \times k_2)$ information bits in an array of k_1 rows and k_2 columns;

2. coding the k_1 rows using code $\mathcal{C}^2$;

3. coding the n_2 columns using code $\mathcal{C}^1$;

The parameters of the product code $\mathcal{P}$ are $n = n_1 \times n_2, k = k_1 \times k_2, \delta = \delta_1 \times \delta_2$, and the code rate R is given by $R = R_1 \times R_2$, where R_i is the code rate of code $\mathcal{C}^i$. Given the procedure used to construct the product code, it is clear that the $(n_2 - k_2)$ last columns of the matrix are codewords of $\mathcal{C}^1$. By using the matrix generator, one can

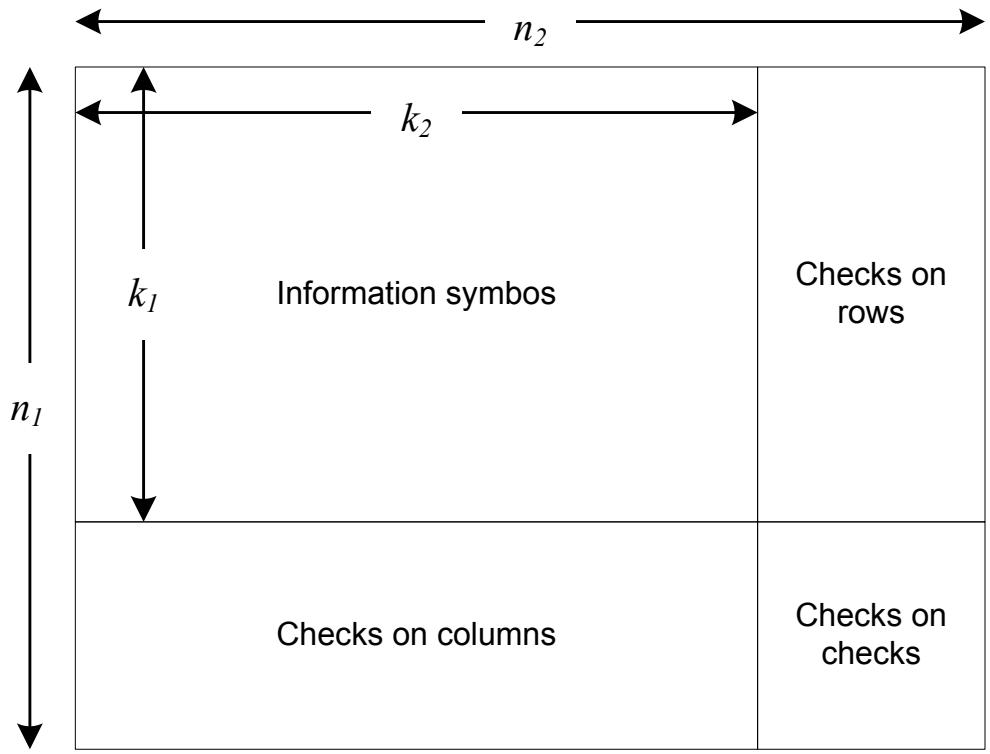

Figure 3.1: Structure of turbo block codes consisting of (k_1, n_1) vertical and (k_2, n_2) horizontal block codes.

show that the $(n_1 - k_1)$ last rows of matrix $\mathcal{P}$ are codewords of $\mathcal{C}^2$. Hence, all of the rows of matrix $\mathcal{P}$ are codewords of $\mathcal{C}^1$ and all of the columns of $\mathcal{P}$ are codewords of $\mathcal{C}^2$.

3.3.2 Turbo Block Code: Decoding

The decoding of turbo block code is performed iteratively as soft extrinsic information is exchanged between the component decoders as explained in [21]. This section mainly refers to the work in [21]. In order to perform the iterative decoding, we need to have soft-in/soft-out decoders for both horizontal and vertical codes. The

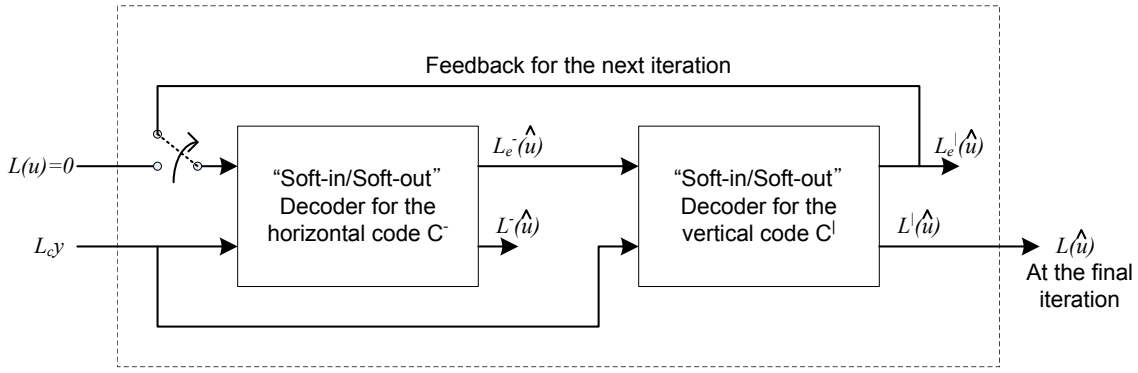

Figure 3.2: Iterative decoding procedure with two "soft-inf/soft-out" decoders with initial $L(u) = 0$, i.e. equally likely source (information) bits

output of the "symbol-by-symbol" maximum *a posteriori* (MAP) decoder is defined as the *a posteriori* log-likelihood ratio for a transmitted "+1" and a transmitted "-1" in the information sequence

$$L(\hat{u}) = L(u \mid \boldsymbol{y}) = \ln \frac{\Pr(u = +1 \mid \boldsymbol{y})}{\Pr(u = -1 \mid \boldsymbol{y})} \tag{3.6}$$

Such a decoder uses *a priori* values $L(u)$ for all information bits u, if available, and channel values $L_c \cdot y$ for all coded bits. It also delivers soft outputs $L(\hat{u})$ on all information bits and an extrinsic information $L_e(\hat{u})$ which contains the soft output information from all the other coded bits in the code sequence and is not influenced by the $L(u)$ and $L_c \cdot y$ values of the current bit. For systematic codes, the soft output for the information bit u will be represented in three additive terms

$$L(\hat{u}) = L_c \cdot y + L(u) + L_e(\hat{u}) \tag{3.7}$$

This means we have three independent estimates for the log-likelihood ratio of the information bits: The channel values $L_c \cdot y$, the *a priori* values $L(u)$ and the values $L_e(\hat{u})$ by a third independent estimator utilizing the code constraint. We do not

have any *a priori* information available for the first iteration, thus we initialize with $L(u) = 0$. Decoding of the horizontal code $\mathcal{C}^-$ starts using the corresponding $L_c \cdot y$ for the information part and for the horizontal parity part. The extrinsic information $L_e^-(\hat{u})$ of the horizontal code $\mathcal{C}^-$ on the information bit u is from Equation (3.7)

$$L_e^-(\hat{u}) = L^-(\hat{u}) - L_c \cdot y. \tag{3.8}$$

This independent estimate on u is now used as the *a priori* value for decoding code $\mathcal{C}^|$ vertically to obtain

$$L_e^|(\hat{u}) = L^|(\hat{u}) - (L_c \cdot y + L(u) + L_e^-(\hat{u})). \tag{3.9}$$

This vertical extrinsic information will be used as new *a priori* value in the subsequent decoding of code $\mathcal{C}^-$ in the next iteration step. The whole procedure is shown in Figure 3.2.

3.3.3 Time-Frequency Turbo Block Code

In this chapter, we propose a time-frequency OFDM turbo block code to achieve low PAPR while maintaining the performance relatively close to the Shannon limit. This scheme is generated when horizontal and vertical codes in a TBC are exploited in frequency and time domain respectively. In Section 2.2.1, we discussed that the physical resource of OFDM system is often defined as a 2-dimensional time-frequency block. The 2-dimensional structure of the output of the TBC output shown in Figure 2.3 is seen as a appropriate form of the OFDM resources as given in Figure 2.4. The row codewords of the TBC output are transmitted using a set of multiple subcarriers in a single OFDM symbol, i.e. by frequency domain. And each column codeword is

transmitted using a single subcarrier of a set of multiple OFDM symbols, i.e. by time domain. To obtain low PAPR, we confine the frequency domain component code to a set of codes with theoretically proven to have good PAPR properties. To improve the BER performance, we utilize powerful linear codes in the time domain.

For the choice of frequency domain component code, we have used the approach proposed in [23, 14] to exploit Golay complementary sequences as the generalized coset for first order Reed-Muller (RM) codes within the second order RM codes. The rationale for using Reed-Muller code is explained enough in Section 3.2.2. Another advantage to use the RM code is that the MAP decoding can be implemented efficiently as given in [24]. Details for the MAP decoding algorithm of the RM code is shown in Appendix A.1.

We still have the question of the code to be selected for time domain component. Although Reed-Muller codes possess the property of having good minimum distance for their affordable code rates, their performance is relatively far from the optimum performance compared to other capacity achieving codes, e.g. turbo codes and LDPC codes. Therefore RM codes, despite their appropriate PAPR properties, are not as efficient as we need performance-wise. To select the time domain component code, the following issues should be taken into account; efficiency in terms of bit error rate (BER) performance, moderate decoding complexity and feasibility of generating soft output. Considering these requirements, Bose-Ray-Chaudhuri (BCH) codes seem as good candidates for time domain component code. This is owing to the fact that turbo block codes using BCH codes as the component codes in both dimensions are reported to perform close to the Shannon limit in [22]. The simplicity of BCH decoder

is also appealing although it only generates hard output. To implement a soft-input soft-output (approximated MAP) decoder for the BCH, the Chase algorithm is used as proposed by [22]. Details for the BCH MAP algorithm is shown in Appendix A.2.

The detailed encoding and decoding of the time-frequency turbo block code with RM and BCH code can be described as follows. Assume that we have the information bit matrix $\mathbf{M}$ such that

$$\boldsymbol{M} = \begin{bmatrix} \boldsymbol{m}_1 \\ \boldsymbol{m}_2 \\ \vdots \\ \boldsymbol{m}_{k_1} \end{bmatrix} = \begin{bmatrix} m_{11} & m_{12} & \cdots & m_{1k_2} \\ m_{21} & m_{22} & \cdots & m_{2k_2} \\ \vdots & \vdots & \ddots & \vdots \\ m_{k_1 1} & m_{k_1 2} & \cdots & m_{k_1 k_2} \end{bmatrix}.$$

Supposed that $\mathrm{RM}_2(1, m)$ is used for frequency component code and $\mathrm{BCH}(n_1, k_1)$ is used for time component code, k_2 is equal to $m + 1$. Using $\mathrm{RM}_2(1, m)$, we encode the message bit sequence $(m_{i1}, m_{i2}, \cdots, m_{i(m+1)})$ to have RM codewords $\boldsymbol{c}_i = (c_{i1}, c_{i2}, \cdots, c_{i2^m})$ for $i = 1, 2, \cdots, k_1$. And using $\mathrm{BCH}(n_1, k_1)$, we encode the message bit sequence $(c_{1j}, c_{2j}, \cdots, c_{k_1 j})$ to make BCH parity bits $(c_{(k_1+1)j}, c_{(k_1+2)j}, \cdots, c_{n_1 j})$ for $j = 1, 2, \cdots, 2^m$. Now we have the matrix $\boldsymbol{C} = [\boldsymbol{d}_1 \ \ \boldsymbol{d}_2 \ \ \cdots \ \ \boldsymbol{d}_{n_1}]^{\mathrm{T}}$, comprising bits of size $n_1 \times 2^m$, where A^{T} is the transpose of the matrix A. We choose a predefined coset representative $\boldsymbol{s} = (s_1, s_2, \cdots, s_{2^m})$ of the form $\sum_{k=1}^{m-1} x_{\pi(k)} x_{\pi(k+1)}$ as given in the Theorem 3.2.2. Note that this predefined coset representative $\boldsymbol{s}$ must be known to both decoder and encoder. Using $\boldsymbol{s}$ we obtain the final sequence $\boldsymbol{d}_i$ in the frequency domain such that $\boldsymbol{d}_i = \boldsymbol{c}_i + \boldsymbol{s}$ for $i = 1, 2, \cdots, n_1$ and form the matrix $\boldsymbol{D} = [\boldsymbol{d}_1 \ \ \boldsymbol{d}_2 \ \ \cdots \ \ \boldsymbol{d}_{n_1}]^{\mathrm{T}}$. Finally, we map each bit of the matrix $\boldsymbol{D}$ to Binary Phase Shift Keying (BPSK) constellation symbols ('0' to '+1' and '1' to '-1') and then map the matrix $\boldsymbol{D}$ consisting of BPSK symbols to the corresponding 2-dimensional block.

Decoding is basically performed iteratively as soft extrinsic information is exchanged between RM and BCH. The decoder receives the real-valued BPSK symbol matrix $\boldsymbol{R}$ of size $n_1 \times 2^m$, such that.

$$\boldsymbol{R} = \begin{bmatrix} \boldsymbol{r}_1 \\ \boldsymbol{r}_2 \\ \vdots \\ \boldsymbol{r}_{n_1} \end{bmatrix} = \begin{bmatrix} r_{11} & r_{12} & \cdots & r_{12^m} \\ r_{21} & r_{22} & \cdots & r_{22^m} \\ \vdots & \vdots & \ddots & \vdots \\ r_{n_1 1} & r_{n_1 2} & \cdots & r_{n_1 2^m} \end{bmatrix}.$$

We assumed that decoder also knows the coset representative $\boldsymbol{s}$ which was used in the encoder. Multiply each row of $\boldsymbol{r}_i = (r_{i1}, r_{i2}, \cdots, r_{i2^m})$ by $(1 - 2 \times \boldsymbol{s})$ using symbol-by-symbol multiplication to have $\boldsymbol{u}_i = \boldsymbol{r}_i \times (1 - 2 \times \boldsymbol{s})$. Now we have $\boldsymbol{U} = [\boldsymbol{u}_1 \ \ \boldsymbol{u}_2 \ \ \cdots \ \ \boldsymbol{u}_{n-1}]^{\mathrm{T}}$. Using matrix $\boldsymbol{U}$, we can perform the iterative decoding procedure as given in Section 3.3.2.

3.4 High Transmission Rate Support

In this section, we provide two methods of increasing the transmission rate of the time-frequency TBC scheme: higher modulation order and higher code rate.

3.4.1 Higher Modulation Order

This section provides a solution to support Quadrature Phase Shift Keying (QPSK) without harming our encoding/decoding structure or any performance degradation of the original time-frequency TBC structure. For completeness, we first give the definition of ZRM, a new family of quaternary RM code. Based on this definition, we can easily observe that the set of codewords of ZRM is a subset of RM codewords.

Definition 3.4.1 *For $r = 0, 1, 2, \cdots, m$, the r^{th} order linear code* $\mathrm{ZRM}_4(r, m)$ *of length 2^m over $\mathbb{Z}_4$ is generated by the monomials in the Boolean functions x_i of degree at most $r-1$ together with two times the monomials in x_i of degree r.*

We have a following theorem given in [25], which defines the transformation from binary RM codes to quaternary RM codes.

Theorem 3.4.1 *For $r = 0, 1, 2, \cdots, m$,* $\mathrm{RM}_2(r, m)$ *of length 2^m is the image under ϕ (Gray mapping) of the quaternary code $ZRM_4(r, m-1)$ of length 2^{m-1} .*

According to Theorem 3.4.1, we can just apply the inverse Gray mapping to each $\mathrm{RM}_2(1, m)$ code in the frequency domain in order to use QPSK symbols. If we shift all n_1 number of $\mathrm{ZRM}_4(1, m-1)$ codewords by a fixed coset representative given by Corollary 3.2.1 and and map each symbol to the constellation by using $\pi/4$ shifted QPSK mapping, i.e. '0' to $(1+i)/\sqrt{2}$, '1' to $(-1+i)/\sqrt{2}$, '2' to $(-1-i)/\sqrt{2}$, and '3' to $(1-i)/\sqrt{2}$, then we still guarantee the 3dB PAPR. We note that the code rate is the same as that of the original BPSK construction, but the transmission rate is doubled.

3.4.2 Higher Code Rate

In this section, we provide a solution to increase the code rate in two different ways. In Section 3.2.2, we saw that there can be $\frac{m!}{2}$ cosets of $\mathrm{RM}_{2^h}(1, m)$ in $\mathrm{RM}_{2^h}(2, m)$ that produce Golay sequences. We might increase the code rate by using multiple cosets rather than using a single coset.

And in the previous section, we increase the modulation order by transforming $\mathrm{RM}_2(r,m)$ to $\mathrm{ZRM}_4(1,m-1)$. And $\mathrm{ZRM}_4(1,m-1)$ codewords are subset of $\mathrm{RM}_4(1,m-1)$ with the following relationship.

$$\mathrm{ZRM}_4(1,m-1)+\sum_{l=1}^{m-1}a_l x_l=\mathrm{RM}_4(1,m-1),\quad a_l\in\{0,1\}$$

We can use this Property to transmit $m-1$ more information bits in the frequency domain codes. The total code rate of the proposed TBC scheme can be up to $\frac{(2m+\lfloor\log_2(\frac{m!}{2})\rfloor)}{2^m}\times\frac{k_1}{n_1}$, where $\lfloor a\rfloor$ is defined as the largest integer which is not greater than a.

3.4.3 Encoding and Decoding

We describe the encoding and decoding procedures in this section. We have the information bit matrix $\mathbf{M}$ such that

$$\boldsymbol{M}=\begin{bmatrix}\boldsymbol{m}_1\\ \boldsymbol{m}_2\\ \vdots\\ \boldsymbol{m}_{k_1}\end{bmatrix}=\begin{bmatrix}m_{11} & m_{12} & \cdots & m_{1k_2}\\ m_{21} & m_{22} & \cdots & m_{2k_2}\\ \vdots & \vdots & \ddots & \vdots\\ m_{k_11} & m_{k_12} & \cdots & m_{k_1k_2}\end{bmatrix}.$$

Here, k_2 is equal to $2m+P$, where $P=\lfloor\log_2(\frac{(m-1)!}{2})\rfloor$. Using $\mathrm{RM}_2(1,m)$, encode $(m_{i1},m_{i2},\cdots,m_{i(m+1)})$ to have binary RM codewords $\boldsymbol{c}_i^{(2)}=(c_{i1}^{(2)},c_{i2}^{(2)},\cdots,c_{i2^m}^{(2)})$ for $i=1,2,\cdots,k_1$. The superscript of $\boldsymbol{c}_i$ denotes the order of the codeword. And then using $\mathrm{BCH}(n_1,k_1)$, encode the bit sequence $(c_{1j}^{(2)},c_{2j}^{(2)},\cdots,c_{k_1j}^{(2)})$ to make BCH parity bits $(c_{(k_1+1)j}^{(2)},c_{(k_1+2)j}^{(2)},\cdots,c_{n_1j}^{(2)})$ for $j=1,2,\cdots,2^m$. Now we have the matrix $\boldsymbol{C}^{(2)}$ comprising binary symbols of size $n_1\times 2^m$. Apply the inverse Gray mapping to every

RM codeword $\boldsymbol{c}_i{}^{(2)}$ for $i = 1, 2, \cdots, n_1$ to have quaternary codeword $\boldsymbol{c}_i{}^{(4)}$ as discussed in Property 1. We assume that we have the table consisting of 2^P coset leaders of the form $\sum_{k=1}^{m-1} x_{\pi(k)} x_{\pi(k+1)}$. The table can be reorganized to maximize the distance between coset leaders. According to the information bits $(m_{i(2m+1)}, \cdots, m_{i(2m+P)})$, choose the corresponding coset leader $\boldsymbol{s}_i^{(4)}$ from the table. And using the remaining information bits $(m_{i(m+2)}, \cdots, m_{i(2m)})$, we obtain the sequence $\boldsymbol{t}_i^{(4)}$ such that $\boldsymbol{t}_i^{(4)} = \sum_{l=1}^{m-1} m_{i(m+1+l)} x_l$, where x_i is the Boolean function of the length 2^{m-1}. For $\boldsymbol{c}_i{}^{(4)}$ with $i > k_1$, we use the pre-fixed $\boldsymbol{s}_i^{(4)} = \boldsymbol{s}_{pre}^{(4)}$ and $\boldsymbol{t}_i^{(4)} = \boldsymbol{t}_{pre}^{(4)}$. At last we obtain the final sequence $\boldsymbol{d}_i^{(4)}$ in the frequency domain such that

$$\boldsymbol{d}_i{}^{(4)} = \boldsymbol{c}_i^{(4)} + 2\boldsymbol{s}_i^{(4)} + \boldsymbol{t}_i^{(4)},$$

and map each quaternary symbol of $\boldsymbol{d}_i^{(4)}$ to the constellation by using $\pi/4$ shifted QPSK mapping as given in Section 3.4.1.

Decoding of the higher transmission rate approach is based on that of the original time-frequency turbo block code scheme with on coset. However, this decoder needs to do extra work in order to detect $2\boldsymbol{s}_i^{(4)}$ and $\boldsymbol{t}_i^{(4)}$. Simply let $\boldsymbol{s}_i^{(2)}$ and $\boldsymbol{t}_i^{(2)}$ be the Gray mapping of $\mathbf{2}s_i^{(4)}$ and $\boldsymbol{t}_i^{(4)}$ respectively. There are $2^{(m-1)+P}$ sequences of $\boldsymbol{s}_i^{(2)} + \boldsymbol{t}_i^{(2)}$ and every sequence is unique. Therefore, we can define $\boldsymbol{u}_x^{(2)}$ in binary symbols $\{-1, 1\}$ to correspond to each sequence of $\boldsymbol{s}_i^{(2)} + \boldsymbol{t}_i^{(2)}$, where $x = 1, 2, \cdots, 2^{(m-1)+P}$. The decoder receives the QPSK symbol matrix $\boldsymbol{R}^{(4)}$ of size $n_1 \times 2^{m-1}$. It first extracts each soft bit from a QPSK symbol by dividing the real part and the imaginary part of the received signal, and place each soft bit to form a two dimensional binary TBC structure $\boldsymbol{R}^{(2)}$ of the size $n_1 \times 2^m$. Using the RM MAP decoder given by [24], we obtain the sequences of Log-Likelihood Ratio (LLR)'s, $\boldsymbol{\Lambda}_i^x$ by considering $\boldsymbol{r}_i^{(2)} \times \boldsymbol{u}_x^{(2)}$ as the input of the

decoder for $i = 1, 2, \cdots, k_1$ and $x = 1, 2, \cdots, 2^{(m-1)+P}$. The most probable sequence $\boldsymbol{u}_{x_i}^{(2)}$ can be obtained by the following equation.

$$x_i = \underset{1 \le x \le 2^{(m-1)+P}}{\arg\max} \sum_{j=1}^{2^m} (\Lambda_{ij}^{x})^2$$

From $\mathbf{\Lambda}_i^{x_i}$ we calculate the most probable extrinsic information and pass it to the BCH soft decoder. We repeat this procedure for the appropriate number of iterations.

3.5 Simulation Result

In order to provide comparative performance evaluation for time-frequency turbo block code, we restrict the frequency domain component code to a first order RM(1,m) code for m = 3, 4, 5, and 6 . For the time domain component code, we consider BCH(63,51). Thus overall code rate for this turbo block code is 0.405, 0.253, 0.152, and 0.089 respectively.

We compare the PAPR to another capacity approaching codes, turbo codes. We examine conventional turbo code which includes two recursive convolutional codes. The turbo code used here is the one in 3GPP2 1X EV-DO standard [26], which is the widely deployed cellular network all over the world. For a fair comparison we set the block length of these codes to $n_1 \times n_2$ (the matrix size in TBC). The transfer function of the turbo code is as follows

$$[1, \frac{1 + D + D^3}{1 + D^2 + D^3}, \frac{1 + D + D^2 + D^3}{1 + D^2 + D^3}]. \tag{3.10}$$

The output of the constituent encoders are punctured or repeated to achieve the same code rates with the TBC scheme.

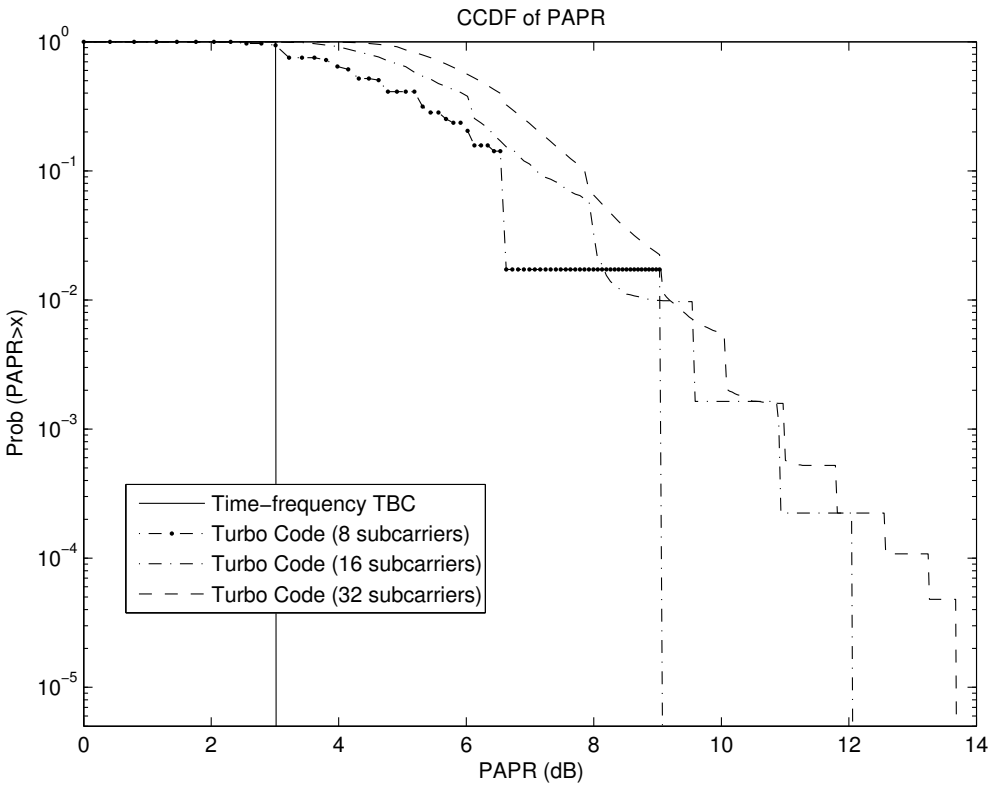

Figure 3.3: Complementary cumulative distribution function of PAPR for various number of subcarriers for BPSK modulation.

Figure 3.3 depicts the complementary cumulative distribution function (ccdf) of PAPR for turbo block coded OFDM and conventional turbo code for OFDM block lengths of the frequency domain component code equal to 8, 16, and 32 respectively, and for the BPSK constellation. For turbo code, we divide the entire coded data block (length $n_1 \times n_2$) into smaller block with the desired length and transmit each sub-block using OFDM. To generate the ccdf, the signal is oversampled by a factor of four. As can be seen in Figure 3.3, the threshold from which the PAPR exceeds with probability of 10^{-5}, has been decreased from 9 dB in turbo code to 3 dB in TBC for the case of 8 subcarriers, which gives 6 dB improvement. For block lengths of 16 and

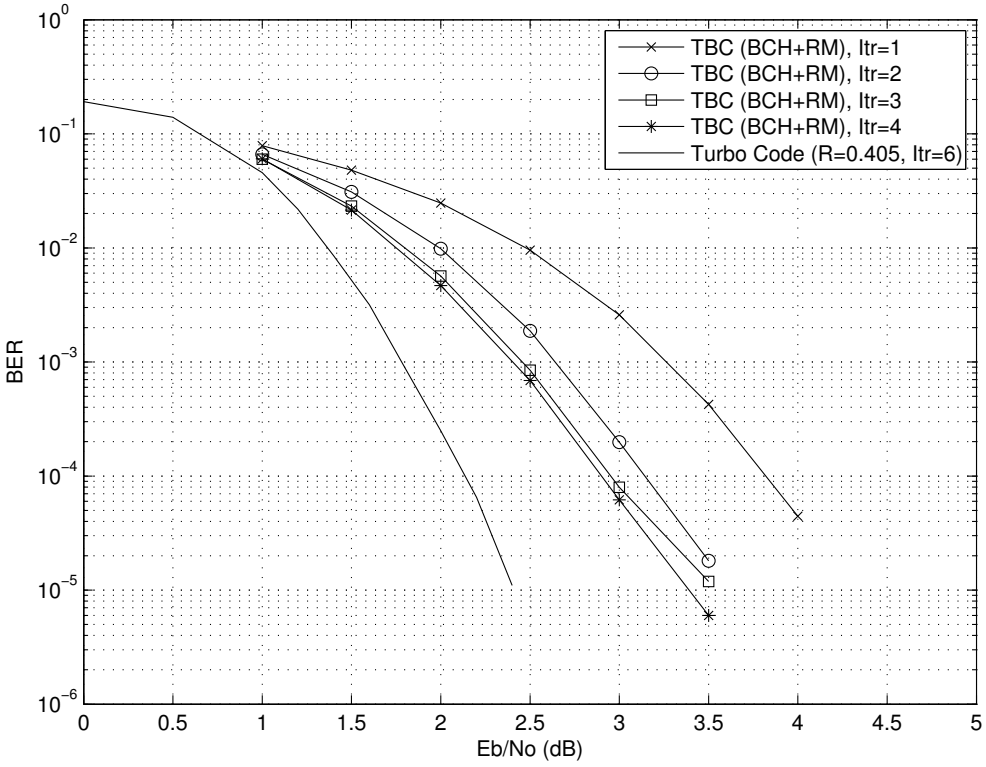

Figure 3.4: Performance comparison of turbo block code (BCH and RM) and convolutional turbo code (number of subcarriers=8, Code rate=0.405)

32 the ccdf is improved by 9 dB and 10.7 dB at probability of 10^{-5}. We should note that this significant improvement in the PAPR distribution is obtained at no extra cost such as decreasing the transmission rate or distorting the transmitted signal. The proposed TBC not only provides a low PAPR but its error correcting capability is also comparable with that of convolutional turbo codes.

Figures 3.4–3.6 present the BER performance of the proposed TBC for the number of subcarriers 8, 16, and 32 respectively under the additive white Gaussian noise (AWGN) channel. Figures are showing BER performance of various decoding iteration numbers up to 4. As expected the performance improves as iterations continue

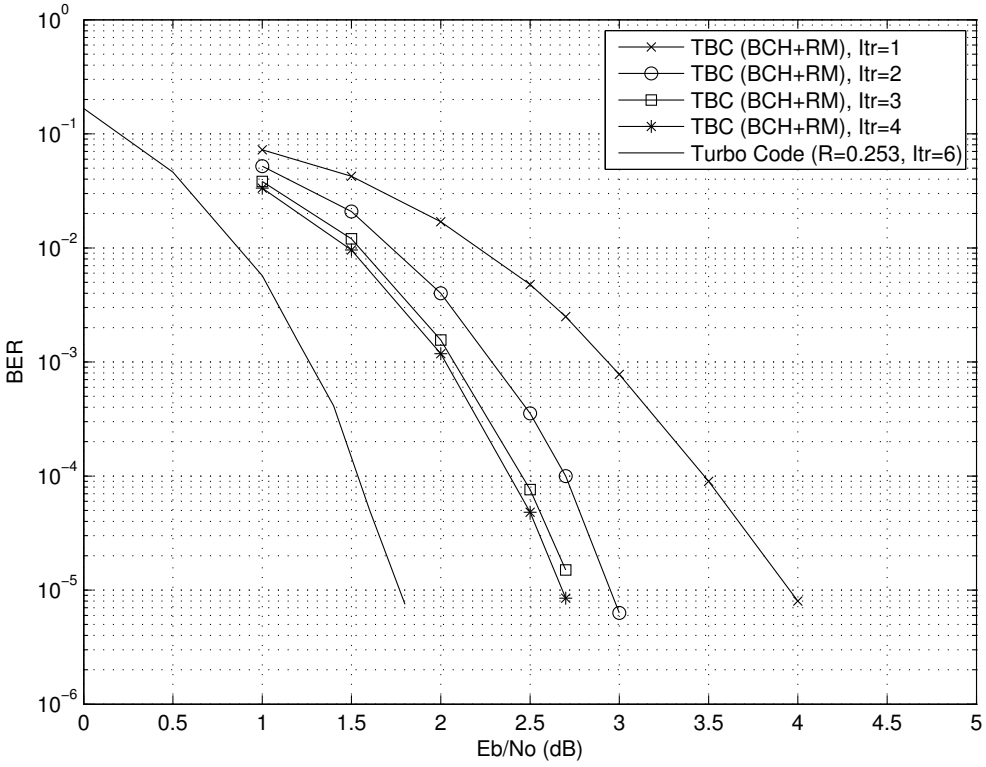

Figure 3.5: Performance comparison of turbo block code (BCH and RM) and convolutional turbo code (number of subcarriers=16, , Code rate=0.253)

and the results converge with 4 iterations. The TBC with the code rate of 0.253 given in Figure 3.5, for which corresponding Shannon limit is -0.81 dB, achieves BER of 10^{-5} at 2.7 dB which is 3.5 dB away from Shannon limit. The performance of the code might seem far from the Shannon limit but we have to note that other capacity achieving codes approach the Shannon limit asymptotically when the code block length goes to infinity. We compare the TBC performance with another capacity approaching code, turbo code with similar block lengths. The performance of the turbo code with the same code rates are also presented in Figures 3.4–3.6. We observe that turbo code outperforms TBC by about 0.9 dB at BER of 10^{-5}. The performance loss

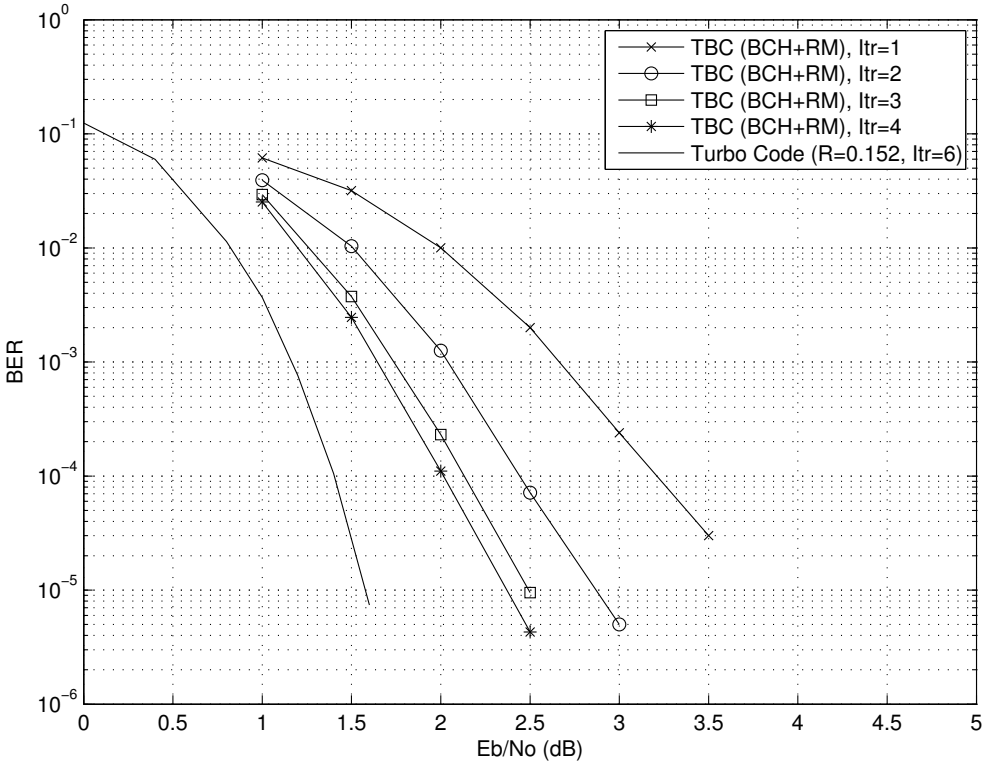

Figure 3.6: Performance comparison of turbo block code (BCH and RM) and convolutional turbo code (number of subcarriers=32, Code rate=0.152)

of the proposed TBC has been compensated for by the significant improvement in PAPR. Table 3.1 summarizes the PAPR and BER performances of both TBC and turbo code, showing the total power gain considering both properties.

We also evaluated the performance of the higher transmission scheme given in Section 3.4. Figure 3.7 depicts the complementary cumulative distribution function (ccdf) of PAPR for time-frequency turbo block coded OFDM and conventional turbo codes for $n_2 = 4,\ 8,\ 16$ and 32 sub-carriers. The PAPR is limited to 3 dB for the proposed scheme so that it has back-off gain of 3dB, 6dB, 8.5dB, and 9dB respectively, over turbo codes. Figures 3.8–3.11 provide BER performance of the turbo code and

Number of sub-carriers	Code rate	PAPR			BER			total gain
		TBC	Turbo	gain	TBC	Turbo	gain	
8 $(m = 3)$	0.405	3 dB	9 dB	6 dB	3.3 dB	2.4 dB	−0.9 dB	5.1 dB
16 $(m = 4)$	0.253	3 dB	12 dB	9 dB	2.7 dB	1.8 dB	−0.9 dB	8.1 dB
32 $(m = 5)$	0.152	3 dB	13.7 dB	10.7 dB	2.4 dB	1.6 dB	−0.8 dB	9.9 dB

Table 3.1: PAPR and BER performance comparison between the time-frequency turbo block code and the conventional Turbo code (BPSK modulation and one single coset assumed)

Number of sub-carriers	Code rates	
	TBC structure with one coset	TBC structure with multiple cosets
4 $(m = 3)$	0.405	0.607
8 $(m = 4)$	0.253	0.455
16 $(m = 5)$	0.152	0.328
32 $(m = 6)$	0.089	0.215

Table 3.2: Supportable code rates of the time-frequency turbo block code with multiple coset supports

the proposed scheme for various number of sub-carriers and code rates. Our scheme has slight performance degradation in the range of 0.5 to 1.7 dB at BER of 10^{-5}. This small loss can be compensated for by the corresponding PAPR gain.

3.6 Summary

In this chapter, we proposed a time-frequency turbo block code solution to the PAPR problem of OFDM systems. To obtain low PAPRs, we restricted the frequency domain component code to the realization of Golay sequences as cosets of the generalized first order Reed-Muller codes. For the time domain components, we selected BCH code due to its appropriate error correcting properties and simplicity of the

Number of sub-carriers	Code rate	PAPR			BER			total gain
		TBC	Turbo	gain	TBC	Turbo	gain	
4 $(m = 3)$	0.607	3 dB	6 dB	3 dB	4.9 dB	3.3 dB	−1.6 dB	1.4 dB
8 $(m = 4)$	0.455	3 dB	9 dB	6 dB	4.4 dB	2.4 dB	−2 dB	4 dB
16 $(m = 5)$	0.328	3 dB	11.5 dB	8.5 dB	3.4 dB	1.8 dB	−1.6 dB	6.9 dB
32 $(m = 6)$	0.215	3 dB	12 dB	9 dB	2.7 dB	1.6 dB	−1.1 dB	7.9 dB

Table 3.3: PAPR and BER performance comparison between the time-frequency turbo block code and the conventional Turbo code (QPSK modulation and maximum possible number of cosets assumed)

decoding. We demonstrated that the proposed TBCs can reduce the PAPRs significantly with a small performance loss compared to best coding schemes with similar rates and block lengths.

The original proposed structure however has limitations of transmission rate. The transmission rate is not high enough in some cases, especially with the large number of subcarriers used. To resolve the limitations, we improved the original time-frequency turbo block code structure to have higher transmission rates. The transmission rate improvement was achieved by introducing the possible mapping binary RM codes to QPSK constellation and by utilizing multiple cosets. The improved rate TBC scheme still showed significant large power gains compared to the conventional turbo codes of the same rates.

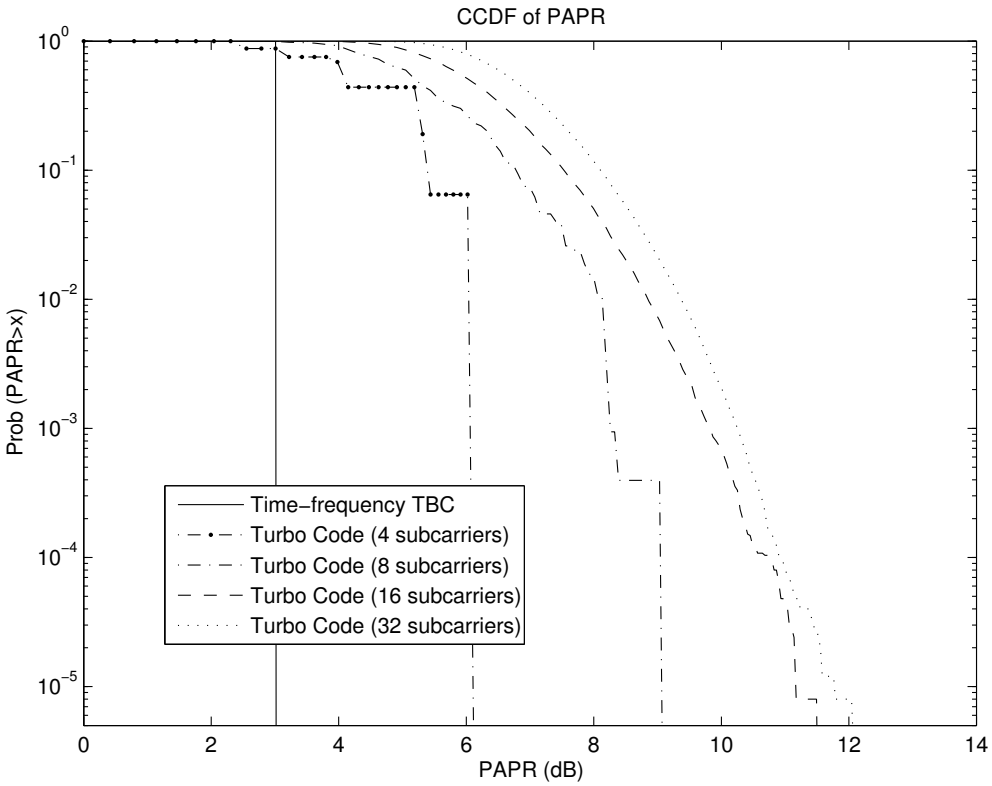

Figure 3.7: Complementary cumulative distribution function of PAPR for various number of subcarriers for QPSK modulation.

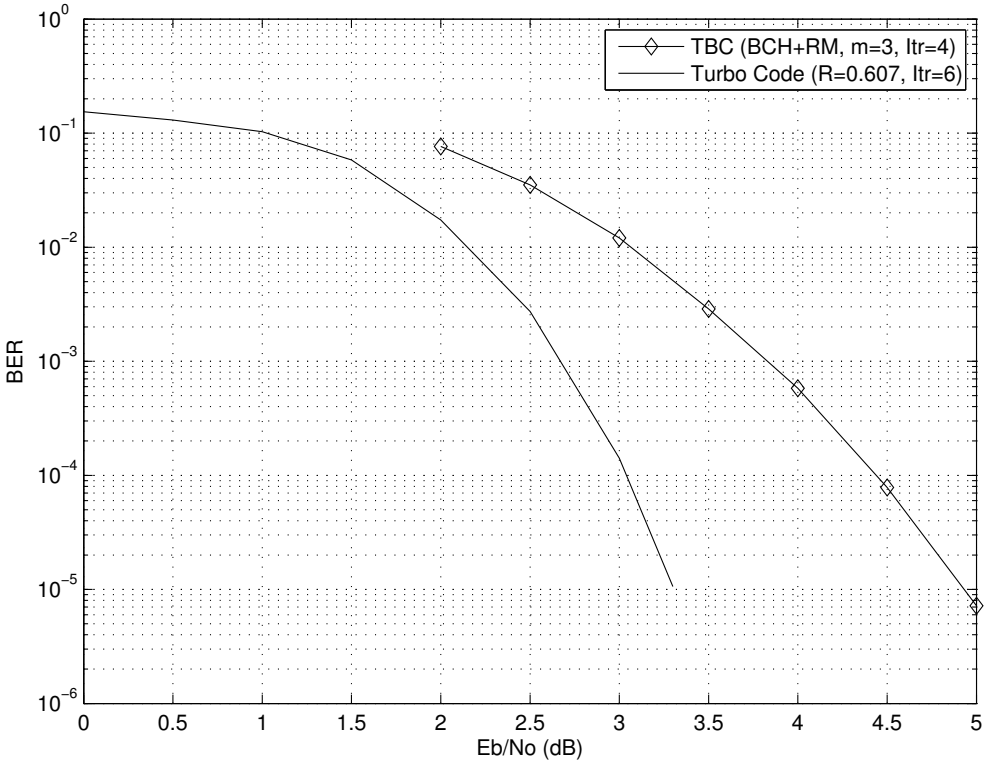

Figure 3.8: Performance comparison of turbo block code (BCH and RM) with multiple cosets and convolutional turbo code (number of subcarriers=4, Code rate=0.607)

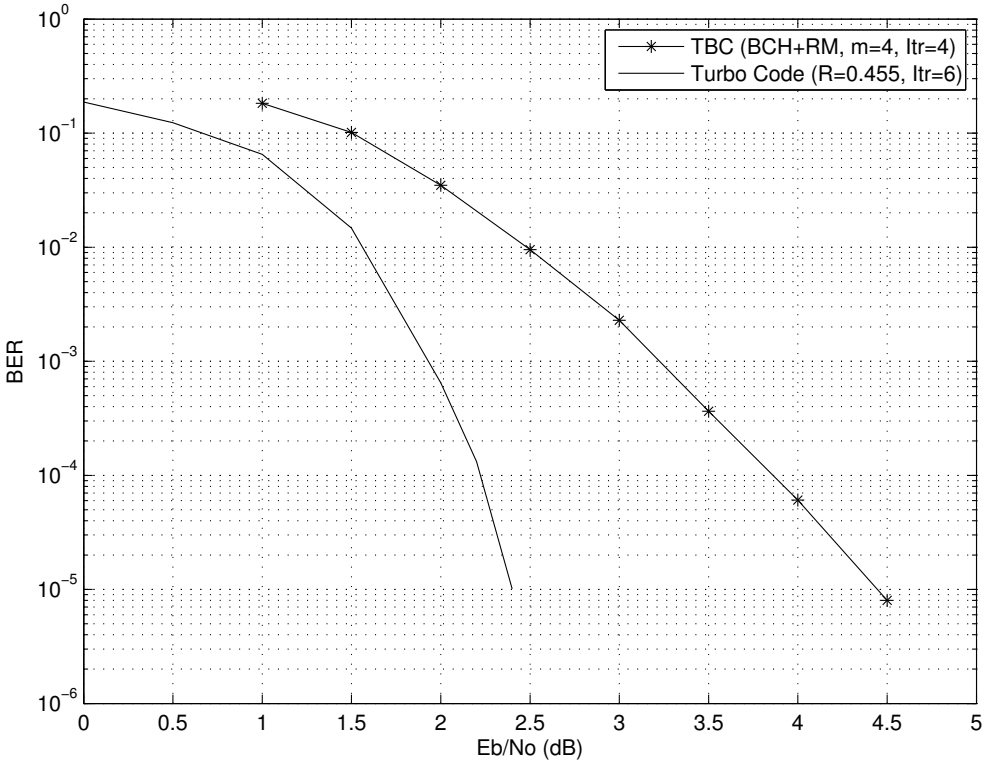

Figure 3.9: Performance comparison of turbo block code (BCH and RM) with multiple coset sand convolutional turbo code (number of subcarriers=8, Code rate=0.455)

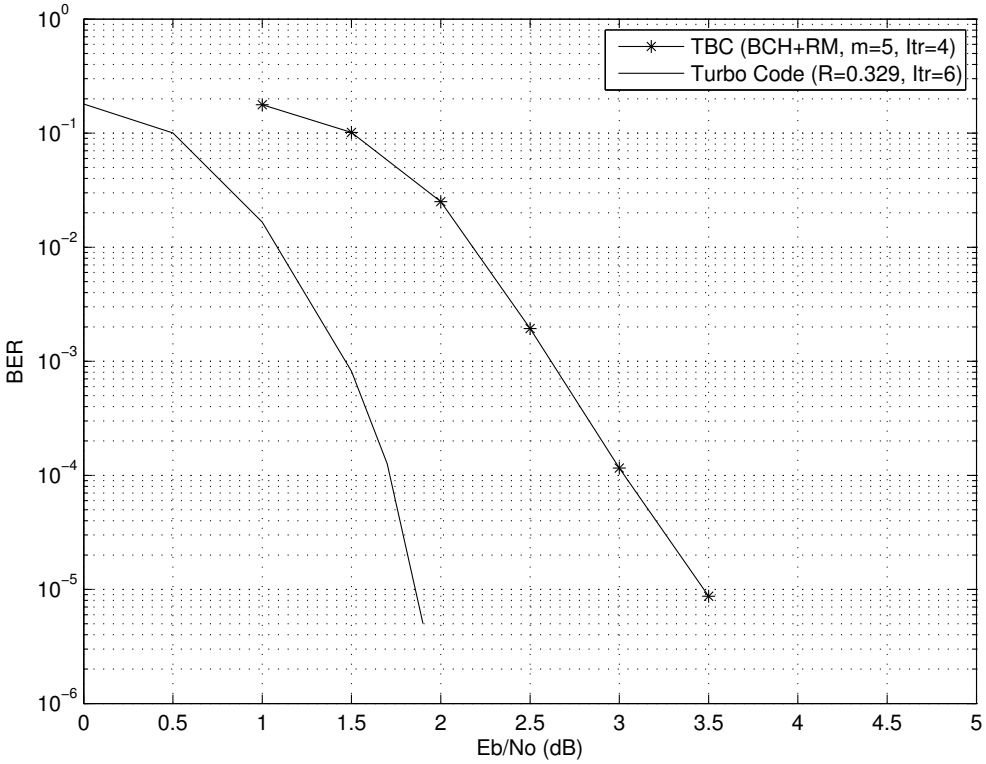

Figure 3.10: Performance comparison of turbo block code (BCH and RM) with multiple cosets and convolutional turbo code (number of subcarriers=16, Code rate=0.328)

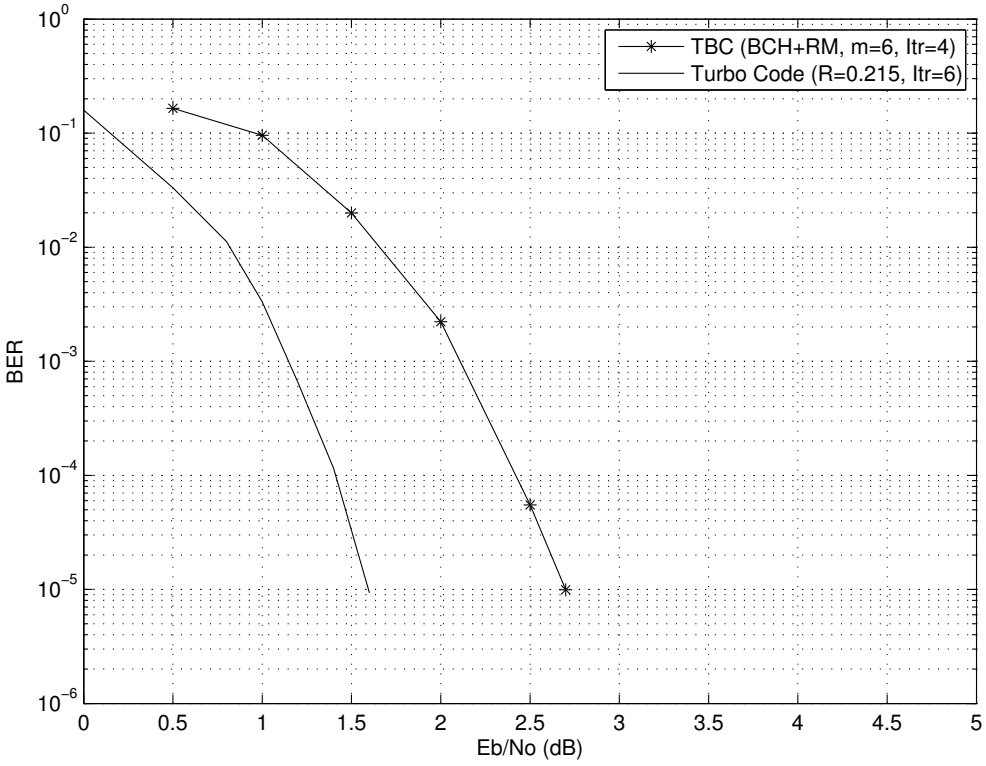

Figure 3.11: Performance comparison of turbo block code (BCH and RM) with multiple cosets and convolutional turbo code (number of subcarriers=32, Code rate=0.215)

Chapter 4

New Codes from Dual BCH Codes

4.1 Introduction

In the previous chapter, we achieved low PAPR for OFDM symbols by using cosets of the generalized first order Reed-Muller codes in turbo block code structure. In this chapter, we investigate another promising frequency domain TBC component code, namely the dual BCH and its modification. The inverse Fourier transform of the codewords of the dual BCH code have low PAPR [12]. Unfortunately no MAP decoder for dual BCH code is known. Therefore we provide the modified dual BCH code such that we preserve PAPR properties while making it amenable to MAP decoding. We will then utilize the modified code in a time-frequency TBC structure. The modified code is employed in frequency component code and BCH is employed in time component code in the TBC. Simulation result shows that our scheme is superior to existing capacity achieving code, e.g. turbo codes.

4.2 PAPR of Dual BCH Codes

The dual of BCH code is known to have low PAPR. Let $\mathbb{F}_q$ be the finite field of size $q = n + 1 = 2^m$ for a positive integer m and β be the n–th root of unity in $\mathbb{F}_q$. The t-error correcting BCH code is generated by the least common multiple of the minimal polynomials of $1, \beta, \beta^2, \cdots, \beta^{2t-1}$ over the field $\mathbb{F}_2$. We denote the dual of the t-error-correcting BCH code of length $n = 2^m - 1$ by DBCH(m, t). In [12], an upper bound is calculated for the peak to mean envelope power ratio (PMEPR) of nonconstant codewords of a DBCH(m, t) as follows

$$U_p = \frac{2^m}{2^m - 1}(2t - 1)^2(\frac{2\ln 2}{\pi}(m + 1) + 2)^2 \tag{4.1}$$

As can be seen for dual BCH codes with similar length, the upper bound depends on the parameter t. We will show using numerical simulation that the upper bound is not tight, nevertheless the dual BCH code has favorable PAPR properties only for $t = 1$.

4.3 New Code Based on Dual BCH Code: Augmented Dual BCH Code

4.3.1 Encoding

Since no simple MAP decoder for dual BCH codes is known, we develop a new code based on dual BCH which is efficiently decodable. This design is not limited to dual BCH codes and can be applied to any code which does not include the all-one vector as a codeword.

Throughout this chapter, message bits, coded bits and received bits are denoted by m_i, c_j and r_j respectively. We also use $\bar{c}$ and $*$ to show the complement (additive inverse) of c and matrix multiplication in $\mathbb{F}_2$ respectively. The set of all codewords is denoted by $\boldsymbol{C}$. We generate a new $(n, k+1)$ code by augmenting (n, k) dual BCH code. We name this new code as augmented dual BCH code. The encoding of augmented dual BCH code is as follows. If the message vector is $(m_0, m_1, \cdots, m_k)$, the codewords of the new code are generated as follows:

$$\boldsymbol{c} = \begin{cases} (m_1, \cdots, m_k) * G_D & \text{for} \quad m_0 = 0 \\ \overline{(m_1, \cdots, m_k) * G_D} & \text{for} \quad m_0 = 1 \end{cases} \tag{4.2}$$

where G_D is the generator matrix of the dual BCH code. The augmented dual BCH code inherits some of the favorable properties of cyclic codes. Specifically, generating codewords or determining whether a vector belongs to $\boldsymbol{C}$ can be accomplished using linear feedback shift registers. The new code also has a minimum distance similar to that of the dual BCH code. Furthermore, the PAPR of the new code is equal to that of the dual BCH code.

4.3.2 Decoding

By generating the codewords as described in Equation (4.2), we can use an approach similar to [24] to decode the received words. The set of all 2^{k+1} codewords, $\boldsymbol{C}$, can be divided into two subsets $\boldsymbol{C}^{m0}$ and $\boldsymbol{C}^{m1}$ whose corresponding message words have $m_0 = 0$ and $m_0 = 1$. Therefore, the elements of $\boldsymbol{C}^{m0}$ and $\boldsymbol{C}^{m1}$ are complement pairwise.

$$\boldsymbol{C} = \boldsymbol{C}^{m0} \cup \boldsymbol{C}^{m1}, \quad \boldsymbol{c}_i^{m0} = \bar{\boldsymbol{c}_i^{m1}} \quad i = 1, \cdots, 2^k \tag{4.3}$$

We construct the matrix $\boldsymbol{D}$ of size $2^k \times n$ such that the i–th row of $\boldsymbol{D}$ is $(1 - 2\boldsymbol{c_i})$ where $\boldsymbol{c_i} \in \boldsymbol{C}^{m0}$, we define the vector $\boldsymbol{L_c}$ such that its i–th element is generated as $L_{c_i} = \Pr(\boldsymbol{r}|\boldsymbol{c}_i) - \Pr(\boldsymbol{r}|\bar{\boldsymbol{c}}_i)$. Interestingly, by multiplying $\boldsymbol{L_c}$ and $\boldsymbol{D}$, we can calculate, for each bit, the summation of probabilities over two subsets of $\boldsymbol{C}$ in which the specific bit is 0 or 1. The i–th component of $\boldsymbol{w} = \boldsymbol{L_c D}$ can be expressed as

$$w_j = \sum_{\boldsymbol{c} \in \boldsymbol{C}_j^0} \Pr(\boldsymbol{r}|\boldsymbol{c}) - \sum_{\boldsymbol{c} \in \boldsymbol{C}_j^1} \Pr(\boldsymbol{r}|\boldsymbol{c}) \tag{4.4}$$

where $\boldsymbol{C}_j^0$ and $\boldsymbol{C}_j^1$ are subsets of $\boldsymbol{C}$ in which the j–th bit is 0 or 1 correspondingly. To calculate this w_j, the value of L_{c_i} has to be available. The probability $\Pr(\boldsymbol{r}|\boldsymbol{c}_i)$ and $\Pr(\boldsymbol{r}|\bar{\boldsymbol{c}}_i)$ can be efficiently calculated by multiplying the log likelihood ratio of the received vector, $\boldsymbol{\lambda}$, by $\boldsymbol{D}^T$. The i–th component of the vector $\boldsymbol{t} = \boldsymbol{\lambda D}^T$ is:

$$t_i = \sum_{j=0}^{j=n-1} [\ln \Pr(r_j|c_{ij}) - \ln \Pr(r_j|\bar{c_{ij}})] \tag{4.5}$$

where c_{ij} is the j–th bit of the i–th codeword. If the value of $s = \sum_{j=0}^{j=n-1} \ln \Pr(r_j|c_{ij}) + \ln \Pr(r_j|\bar{c_{ij}})$ is available, considering Equation (4.5), $\Pr(\boldsymbol{r}|\boldsymbol{c}_i)$ and $\Pr(\boldsymbol{r}|\bar{\boldsymbol{c}}_i)$ can be easily generated as

$$\begin{aligned} \ln \Pr(\boldsymbol{r}|\boldsymbol{c}_i) &= \frac{s + t_i}{2} \\ \ln \Pr(\boldsymbol{r}|\bar{\boldsymbol{c}}_i) &= \frac{s - t_i}{2} \end{aligned} \tag{4.6}$$

We also note that once $\boldsymbol{\lambda}$ is available, the calculation of $\ln \Pr(r_j|0)$ and $\ln \Pr(r_j|1)$ is straightforward.

LLR is simply calculated from w_j. By Baye's rule, Equation (4.4) is changed to

the following equation.

$$\begin{aligned} w_j &= \sum_{\boldsymbol{c}\in\boldsymbol{C}_j^0} \frac{\Pr(\boldsymbol{c}|\boldsymbol{r})\Pr(\boldsymbol{r})}{\Pr(\boldsymbol{c})} - \sum_{\boldsymbol{c}\in\boldsymbol{C}_j^1} \frac{\Pr(\boldsymbol{c}|\boldsymbol{r})\Pr(\boldsymbol{r})}{\Pr(\boldsymbol{c})} \\ &= 2^k \Pr(\boldsymbol{r})[\sum_{\boldsymbol{c}\in\boldsymbol{C}_j^0} \Pr(\boldsymbol{c}|\boldsymbol{r}) - \sum_{\boldsymbol{c}\in\boldsymbol{C}_j^1} \Pr(\boldsymbol{c}|\boldsymbol{r})] \\ &= 2^k \Pr(\boldsymbol{r})[\Pr(c_j = 0|\boldsymbol{r}) - \Pr(c_j = 1|\boldsymbol{r})] \end{aligned} \tag{4.7}$$

The constant factor $2^k \Pr(\boldsymbol{r})$ can be computed similarly:

$$\begin{aligned} q &= \sum_{\boldsymbol{c}\in\boldsymbol{C}_j^0} \Pr(\boldsymbol{r}|\boldsymbol{c}) + \sum_{\boldsymbol{c}\in\boldsymbol{C}_j^1} \Pr(\boldsymbol{r}|\boldsymbol{c}) \\ &= 2^k \Pr(\boldsymbol{r})[\sum_{\boldsymbol{c}\in\boldsymbol{C}_j^0} \Pr(\boldsymbol{c}|\boldsymbol{r}) + \sum_{\boldsymbol{c}\in\boldsymbol{C}_j^1} \Pr(\boldsymbol{c}|\boldsymbol{r})] \\ &= 2^k \Pr(\boldsymbol{r})[\Pr(c_j = 0|\boldsymbol{r}) + \Pr(c_j = 1|\boldsymbol{r})] \\ &= 2^k \Pr(\boldsymbol{r}) \end{aligned} \tag{4.8}$$

Finally, we can obtain log likelihood ratio (LLR):

$$\mathrm{LLR}_j = \ln \frac{\Pr(c_j = 0 \mid \boldsymbol{r})}{\Pr(c_j = 1 \mid \boldsymbol{r})} = \ln \frac{1 + w_j/q}{1 - w_j/q} \tag{4.9}$$

4.3.3 TBC with Augmented Dual BCH Code

Using the soft decoder developed in Section 4.3.2, we can utilize the augmented dual BCH code as the frequency component code of time-frequency turbo block code with low PAPR. The TBC encoding and decoding are given in Section 3.3. We denote the message length of the time domain constituent code and the frequency domain constituent code by k_1 and k_2 and the code block lengths by n_1 and n_2. The codes have corresponding rates of $R_1 = \frac{k_1}{n_1}$ and $R_2 = \frac{k_2}{n_2}$ respectively for time and frequency domain codes and the TBC code rate is $R = R_1 \times R_2$. We employ the augmented

dual BCH code (See Section 4.3.1) as the frequency domain component code. We use BCH code as the time domain component code as motivated in Section 3.3.3. We note that the PAPR bound of the dual BCH code in Section 4.2 is only valid for the nonconstant codewords. There are two constant codewords in the augmented dual BCH code, all-zero and all-one sequences. All-zero codeword is made by the encoding of all-zero message, $000\cdots0$, and all-one codeword is made by the encoding of all-zero message with the exception of the first bit, $100\cdots0$. By fixing the last message bit as '1', we can avoid the constant codewords of the augmented dual BCH code. This reduces the code rate to $R = \frac{k_1(k_2-1)}{n_1 n_2}$ but guarantees low PAPR.

4.4 Simulation Results

In this section, we evaluate the efficiency of the proposed turbo block coded OFDM system based on the new code proposed in Section 4.3. The TBC encoding is performed according to the method given in Section 4.3.3. As mentioned in Section 4.2, among dual BCH codes only those with $t = 1$ have appealing PAPR properties. This is depicted in Figure 4.1, where complementary cumulative distribution function (ccdf) of PAPR for dual BCH codes with $m = 4, 5$, and 6 are given. The maximum PAPR for these codes with $t = 1$ are respectively 5.4, 6.0, and 6.3 dB and the length of these codes are respectively 15, 31, and 63 ($n_2 = 2^m - 1$). As the parameter t increases from 1 to 2, the maximum PAPR grows by 3.7, 5.5, and 5.5 dB respectively for $n_2 = 15$, 31, and 63. To illustrate the effect of the growth of t on PAPR, for $n_2 = 63$ the PAPR is presented for $t = 11$. As discussed above, we use augmented DBCH(m,1), denoted by A-DBCH(m,1) in the frequency domain and the BCH code

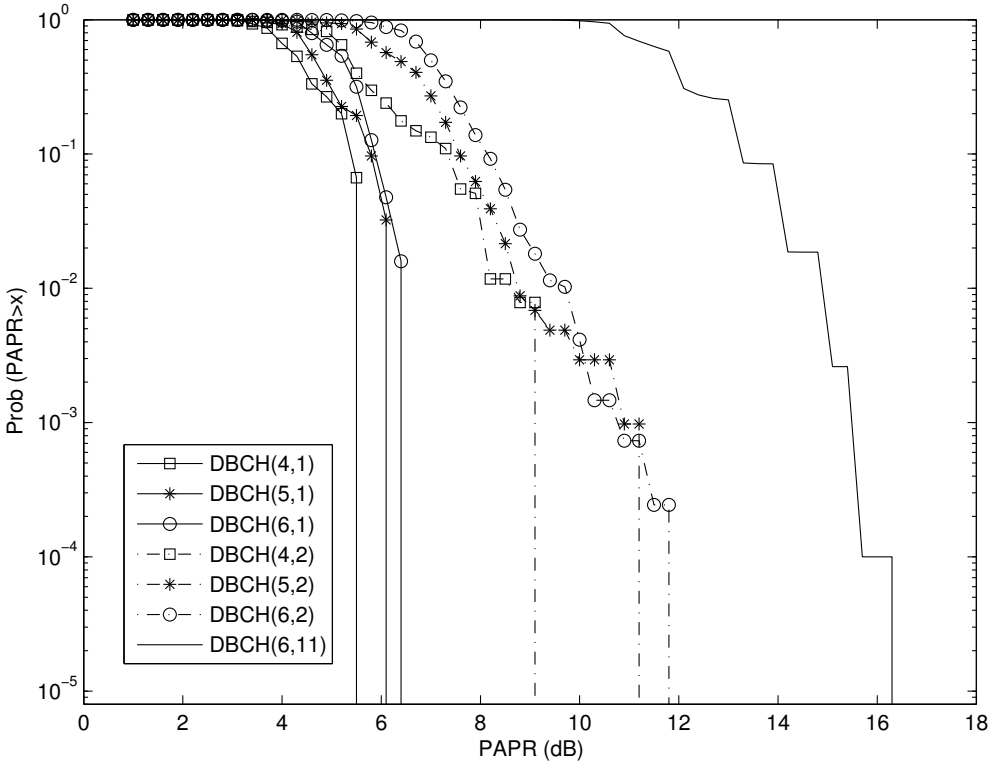

Figure 4.1: CCDF of PAPR for dual BCH codes for different values of t. $n_2 = 63$: marked with circles, $n_2 = 31$: marked with stars, $n_2 = 15$: marked with squares.

in the time domain.

We compare the performance and PAPR of these codes with a capacity achieving code, namely turbo code given in Section 3.5. To match the block size between TBC and turbo code, coded blocks of the turbo code are truncated into smaller blocks of length $2^m - 1$ which are transmitted as OFDM symbols. Figure 4.2 compares the ccdf of PAPR of both codes. The constellation is BPSK and the signals are four times oversampled. As can be seen, the proposed turbo block coded OFDM scheme provides respectively 6.4 and 7.5 dB lower PAPRs for $m = 4$ and 5. This significant improvement does not come at the expense of any distortion or any reduction in the

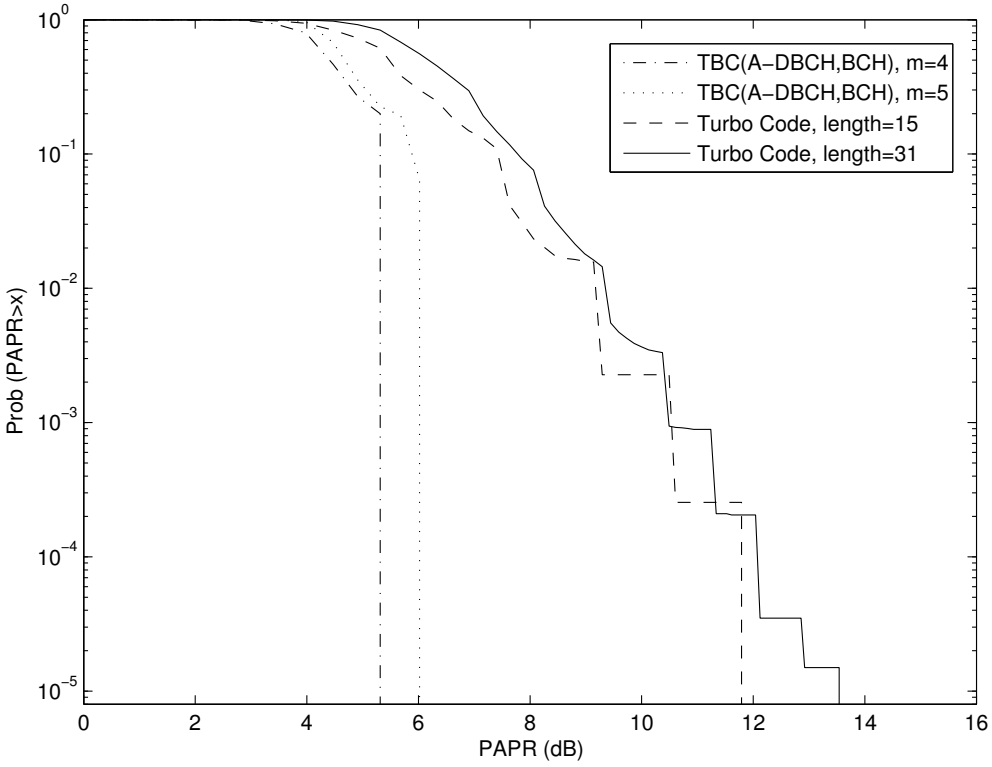

Figure 4.2: PAPR comparison of turbo block code and conventional turbo code.

bandwidth.

Figure 4.3 presents the performance of the proposed turbo block coded OFDM scheme. The overall block lengths of TBC are respectively 945 and 1953 for $m = 4$ and $m = 5$ respectively and corresponding code rates are $R = 0.241$ and 0.146. In the simulation, we use 4 iterations between the two constituent decoders. For comparison, we also give the performance of the turbo code with the same lengths and the same code rates as the TBC scheme. As presented, the performance of the proposed system is 1.5 and 2.0 dB worse than turbo code for $m = 4$ and $m = 5$ respectively. It is noteworthy that for large OFDM block lengths there is a tradeoff

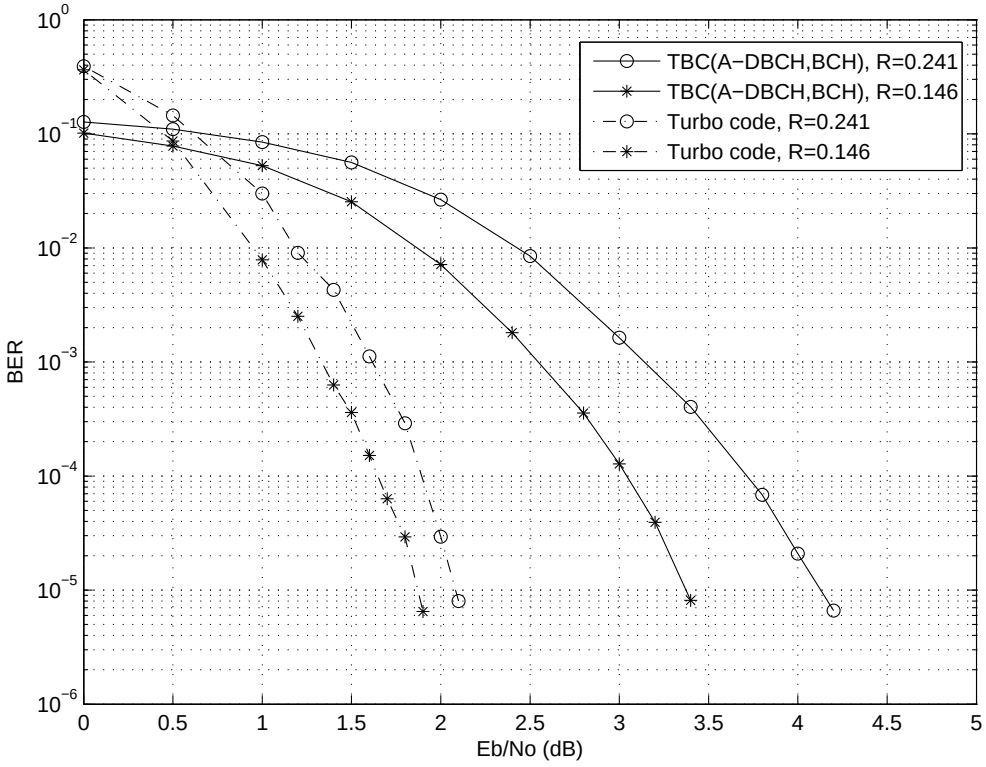

Figure 4.3: Performance comparison of turbo block code and turbo code, $n_1 = 63$, $n_2 = 15$: marked with circles , $n_1 = 63$, $n_2 = 31$: marked with stars.

between the code rate and PAPR of the proposed scheme. By increasing t, both code rates and PAPRs increase as a function of t.

Table 4.1 summarizes the performance of the proposed scheme compared to the conventional turbo code. From the table, we observe that TBC scheme with augmented dual BCH in frequency domain and BCH in time domain gives respectively 4.5 dB and 5.9 dB gains over the conventional turbo code for $m = 4$ and $m = 5$.

Number of sub-carriers	Code rate	PAPR			BER			total gain
		TBC	Turbo	gain	TBC	Turbo	gain	
15 $(m = 4)$	0.241	5.4dB	11.8dB	6.4dB	4.1dB	2.1dB	−2.0dB	4.4dB
31 $(m = 5)$	0.146	6.0dB	13.5dB	7.5dB	3.4dB	1.9dB	−1.5dB	6.0dB

Table 4.1: PAPR and BER performance comparison between the DBCH-BCH turbo block code (TBC) and the conventional Turbo code

4.5 Summary

In this chapter, we constructed an augmented code based on dual BCH code that is amenable to MAP decoding. Since the PAPRs of the codewords of the augmented dual BCH code are the same as those of a dual BCH code. We have utilized this code as the frequency domain constituent code in a time-frequency turbo block coded OFDM system. We have shown that the proposed scheme achieves significantly lower PAPR at the cost of small performance degradation compared to best known capacity achieving codes.

Chapter 5

Probabilistic Low PAPR Coded OFDM

5.1 Introduction

In Chapter 2, we introduced a few PAPR reduction approaches including selected mapping (SLM) or partial transmit signaling (PTS) [3] [4]. In these methods, the probability of occurring large PAPR signals is decreased by generating alternative signals carrying the same information and transmitting the best one in terms of PAPR. However, the explicit transmission of side information regarding the selected signal is crucial for the receiver to recover the signal properly. The embedding of the side information in the data sequence may cause PAPR regrowth, reduce the bandwidth efficiency or cause performance loss due to the potential of receiving erroneous side information. Alternatively, we might use dedicated channels to assure the side information is protected by a powerful code, but this may increase the de-

lay and the complexity of the system. In this chapter, we design a coded OFDM system with reduced PAPR which does not require transmission of side information and performs sufficiently close to the capacity achieving codes. We seek a method with the feasibility of accommodating arbitrary code rates and block lengths and arbitrary constellation per subcarrier. By incorporating the probabilistic and coding approaches, We develop a method which satisfies the aforementioned requirements. We exploit random sequences to reduce the PAPR. At the decoder, we recover both the transmitted data and the selected random sequence.

5.2 Probabilistic Approaches in Coding for PAPR Reduction

To develop a PAPR reduction coding method with good performance, we start with a capacity achieving code such as turbo code consisting of two convolutional codes. The equiprobable and i.i.d. data bits are first encoded by the turbo code and then mapped to symbols a_n selected from a BPSK constellation. The modulated symbols compose blocks of length of N OFDM symbols denoted by: $\boldsymbol{a} = [a_1 \;\; a_2 \;\; \cdots \;\; a_N]$.

5.2.1 Encoding

To reduce the PAPR, We seek a probabilistic approach based on random sequences. By multiplying the data block by s independent and randomly generated sequences $\boldsymbol{q}^s = [q_1^s q_2^s \cdots q_N^s]$, s alternative blocks carrying the same information are generated as $\boldsymbol{a^s} = \boldsymbol{a} * \boldsymbol{q^s}$ where $*$ stands for element-by-element multiplication. The

criterion to select the signal for transmission is to exhibit the lowest PAPR

$$\boldsymbol{a}^t = \arg \min_{1<s<S} PAPR\ \{IFFT(\boldsymbol{a}^s)\}, \tag{5.1}$$

where $IFFT(\boldsymbol{a})$ is the inverse fast fourier transform of the vector $\boldsymbol{a}$ and $PAPR(\boldsymbol{a})$ is the PAPR of the sequence $\boldsymbol{a}$. The set of all random sequences is known to both the transmitter and the receiver. However no explicit information regarding the selected sequence is exchanged between the two sides.

5.2.2 Decoding

The selected random sequence is determined in the first iteration where the first constituent code is decoded using the information of s different random sequences. Thereby, the metrics of the Bahl-Cocke-Jelinek-Raviv (BCJR) algorithm developed in [27] are calculated as follows:

$$\begin{aligned} \alpha_{l+1}^s(t') &= \sum_{t=1}^{T-1} \alpha_l^s(t)\gamma_l^s(t,t'), \\ \beta_l^s(t) &= \sum_{t'=0}^{T-1} \gamma_l^s(t,t')\beta_{l+1}^s(t'), \\ \gamma_l^s(t,t') &= \frac{1}{(2\pi\sigma^2)^{\frac{n}{2}}} \exp[\frac{-1}{2\sigma_2}|\boldsymbol{r}_l - \boldsymbol{a}^{(t,t')}\boldsymbol{q}^s|^2]\Pr(x_t = x^{(t,t')}). \end{aligned} \tag{5.2}$$

The details of the above Equations can be found in [28].

For simplicity of the decoding algorithm, we assume that we transmit all-zero codewords without loss of generality. Eventually, the decoder generates s sets of log-likelihood ratios (LLR), each corresponding to a random sequence as follows:

$$\boldsymbol{\lambda^s} = [\lambda_1^s \lambda_2^s \cdots \lambda_N^s] \tag{5.3}$$

To detect the random sequence, we maximize $\Pr(\boldsymbol{q}^i|\boldsymbol{\lambda}^1, \boldsymbol{\lambda}^2, \cdots, \boldsymbol{\lambda}^s)$ which is equivalent to:

$$\hat{\boldsymbol{q}} = \arg \max_{\boldsymbol{q}^i, 1 \leq i \leq S} f(\boldsymbol{\lambda}^1, \boldsymbol{\lambda}^2, \cdots, \boldsymbol{\lambda}^s|\boldsymbol{q}^i) \tag{5.4}$$

where $\hat{\boldsymbol{q}}$ denotes the detected random sequence in the receiver. The joint probability density function of LLRs can be expressed as:

$$f(\boldsymbol{\lambda}^1, \boldsymbol{\lambda}^2, \cdots, \boldsymbol{\lambda}^S|\boldsymbol{q}^i) = \prod_{s=1}^{S} f(\boldsymbol{\lambda}^s|\boldsymbol{q}^i) \tag{5.5}$$

The distribution of the output LLR of the BCJR algorithm can be well approximated by a consistent Gaussian [29]. In a consistent Gaussian distribution, the variance is twice the absolute value of the mean. In other words, one parameter is enough to describe the distribution,

$$f(\boldsymbol{\lambda}^s|\boldsymbol{q}^i) = \prod_{j=1}^{N} \frac{1}{\sqrt{2\pi\sigma^2}} \exp \frac{-(\lambda_j^s - \bar{m})^2}{4\bar{m}} \tag{5.6}$$

When the random sequence utilized in the decoder is the one used in the transmitter, we show the mean of $f(\boldsymbol{\lambda}^i|\boldsymbol{q}^i)$ by $\bar{m} = m$. Correspondingly, the mean of $f(\boldsymbol{\lambda}^j|\boldsymbol{q}^i)$ for $j \neq i$ is denoted by m'. We note that $m \gg m'$. Maximizing $f(\boldsymbol{\lambda}^1, \boldsymbol{\lambda}^2, \cdots, \boldsymbol{\lambda}^S|\boldsymbol{q}^i)$ for $1 \leq i \leq S$ is equivalent to minimizing L_i defined as:

$$L_i = \sum_{s=1, s\neq i}^{S} \sum_{j=1}^{N} \frac{|\lambda_j^s|^2}{m'} + \sum_{j=1}^{N} \frac{|\lambda_j^i|^2}{m} \tag{5.7}$$

Since $m' \ll m$, to minimize L_i we have to maximize $\sum_{j=1}^{N} |\lambda_j^i|^2$. Hence the selected random sequence is determined as:

$$\hat{\boldsymbol{q}} = \arg \max_{\boldsymbol{q}^i, 1 \leq i \leq S} \sum_{j=1}^{N} |\lambda_j^i|^2 \tag{5.8}$$

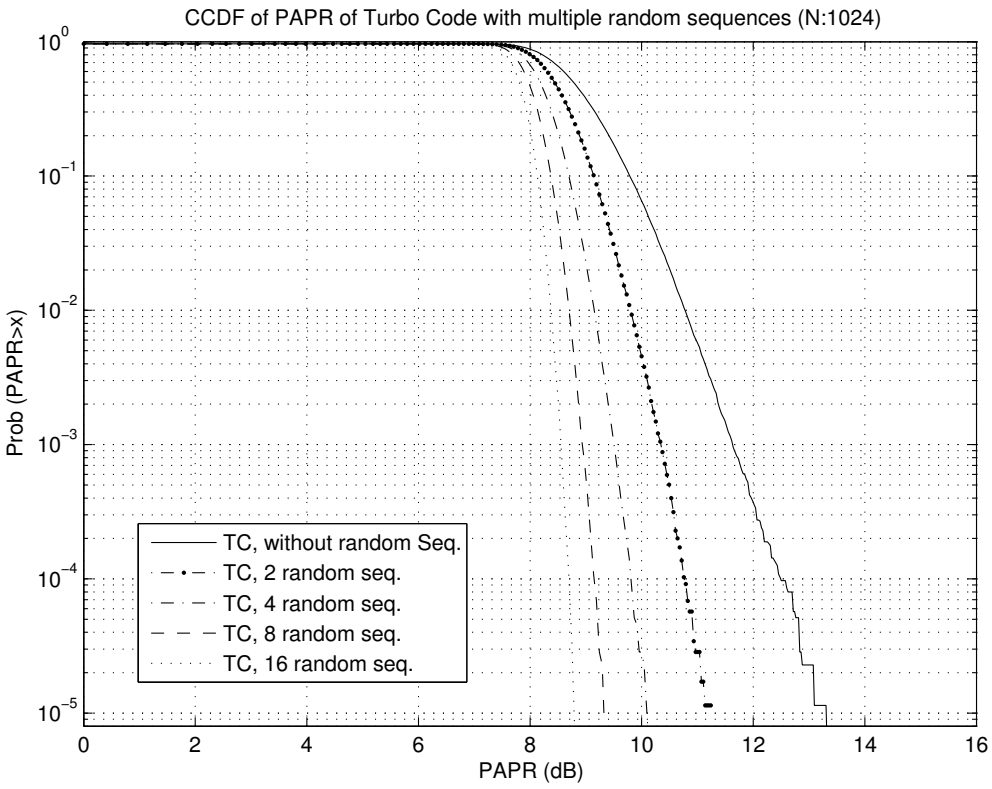

Figure 5.1: Complementary cumulative distribution function of PAPR for turbo code with various number of random sequences. (N=1024)

5.3 Simulation Results

In this section, we demonstrate the efficiency of the proposed method in obtaining a low PAPR near Shannon limit coded OFDM system. We consider a parallel concatenated turbo code [26] with rate $R = \frac{1}{3}$ and coded block length of $N = 1024$ and $N = 2048$. The exact coding rate is not exactly equal to $\frac{1}{3}$ and is 0.375 and 0.372 respectively. This is because the number of subcarriers is a power of two. This rate matching was performed by puncturing a certain number of coded symbols. The requirement of the power of two for the coded block length is in order to have faster

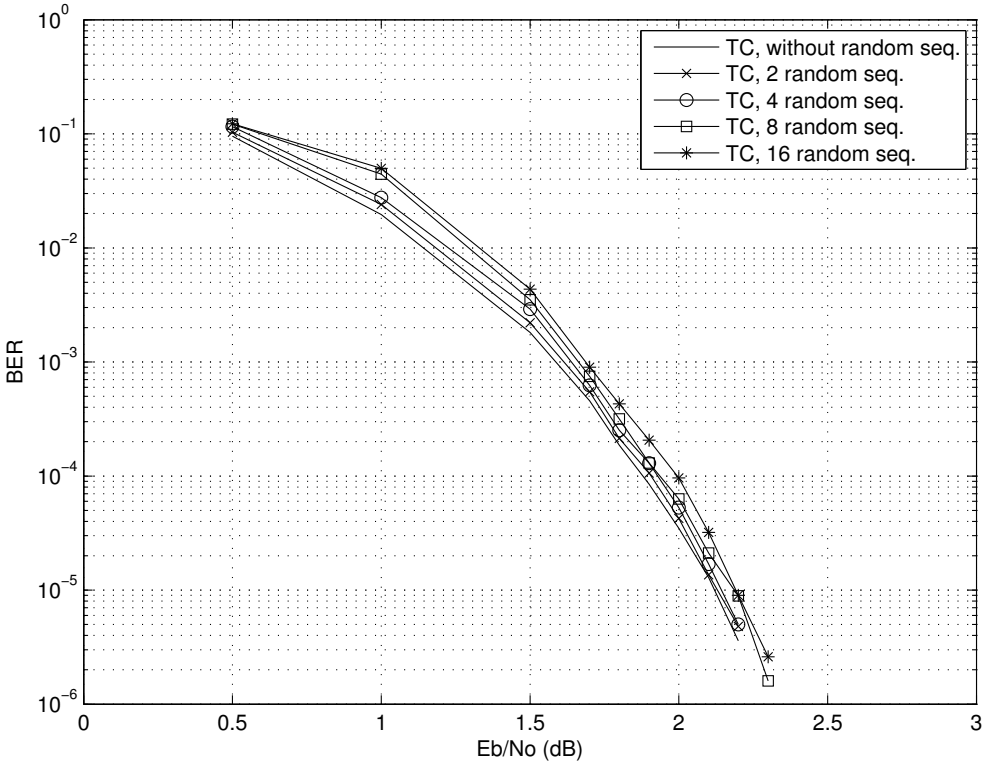

Figure 5.2: Performance comparison of turbo code with various number of random sequences. (N=1024)

FFT/IFFT implementation. The constituent codes are two recursive systematic convolutional code with the following transfer functions:

$$[1, \frac{1+D+D^3}{1+D^2+D^3}, \frac{1+D+D^2+D^3}{1+D^2+D^3}]. \tag{5.9}$$

The transmitter selects the best signal as described in (5.8) when $S = 2, 4, 8$ and 16 random sequences are utilized. The complementary cumulative distribution function (ccdf) of PAPR is depicted in Figure 5.1 and 5.3 for $N = 1024$ and $N = 2048$ respectively. The constellation is BPSK and signals are four times oversampled. As can be seen the Figure 5.1, we are able to reduce the PAPR by 2.1, 3.1, 4.0 and 4.6 dB

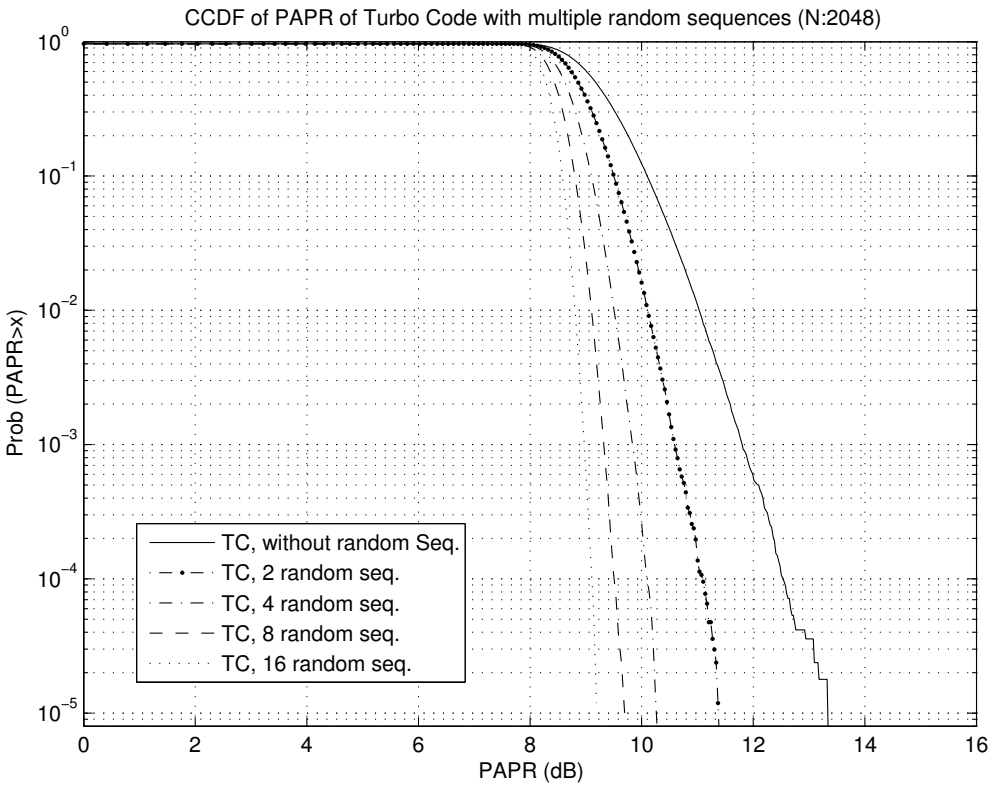

Figure 5.3: Complementary cumulative distribution function of PAPR for turbo code with various number of random sequences. (N=2048)

by using 2, 4, 8 and 16 random sequences for $N = 1024$. Figure 5.3 shows that the proposed scheme has PAPR gains of 2.0, 3.0, 3.6 and 4.2 dB by using 2, 4, 8 and 16 random sequences respectively for $N = 2048$. Figure 5.2 and Figure 5.4 compare the performance of the system with and without random sequences over additive white Gaussian noise (AWGN) channel for $N = 1024$ and $N = 2048$ respectively. From the figures, we can see that the difference between the performance for $S = 2, 4, 8$ and 16 is at most 0.2 dB which is negligible for both block lengths. As presented, the significant PAPR decrease is obtained at the expense of a slightly higher decoding complexity and a negligible performance degradation around 0.05–0.2dB compared to

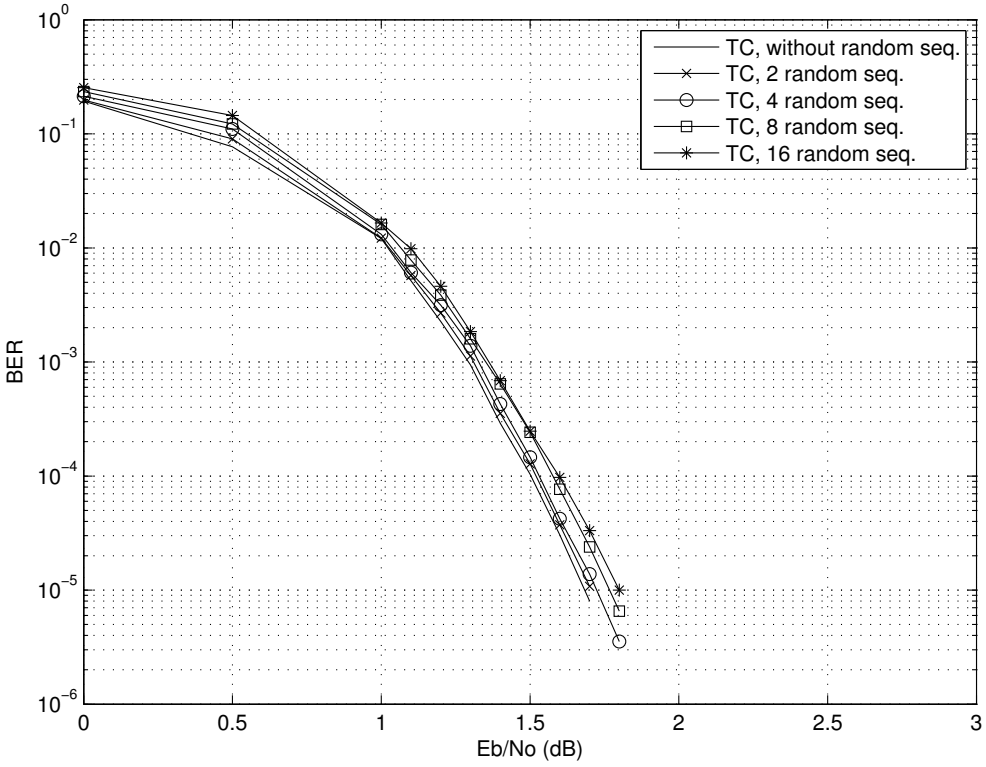

Figure 5.4: Performance comparison of turbo code with various number of random sequences. (N=2048)

the case when no random sequence is used. It is noteworthy that the performance of the system, when the selected random sequence is determined through the decoding process, is exactly similar to the case that perfect side information regarding the random sequence is transmitted to the receiver especially for the high SNR scenarios.

Table 5.1 summarizes the total gain of the proposed scheme. PAPR gain (BER loss) is the PAPR (BER) difference of the turbo code using the number of random sequences compared to the turbo code without using random sequences. Considering both PAPR gain and BER loss, the total power gain ranges from 2 dB to 5 dB depending on the number of random sequences and the number of subcarriers which

Number of sub-carriers	Code Rates	Number of Sequences	PAPR gain	BER loss	Total gain
1024	0.375	2	2.1 dB	−0.05 dB	2.05 dB
		4	3.1 dB	−0.05 dB	3.05 dB
		8	4.0 dB	−0.15 dB	3.95 dB
		16	4.6 dB	−0.15 dB	4.45 dB
2048	0.372	2	2.0 dB	−0.05 dB	1.95 dB
		4	3.0 dB	−0.1 dB	2.9 dB
		8	3.6 dB	−0.15 dB	3.45 dB
		16	4.2 dB	−0.2 dB	4.0 dB

Table 5.1: PAPR and BER performance comparison between the time-frequency turbo block code and the conventional turbo code (QPSK modulation and maximum possible number of cosets assumed)

is identical to the block length.

5.4 Summary

For any code book, amenable to MAP decoding, we proposed a PAPR reduction method which shifts the PAPR ccdf of original system to the left. We applied this method to a capacity achieving code, namely turbo code and have shown performance close to Shannon limit with significant low PAPRs. In this method, the PAPR is decreased significantly while the performance degradation is only less than 0.2 dB from that of a capacity achieving code. This method can be flexibly applied for arbitrary constellation per subcarrier, arbitrary code books and code rates, and any number of subcarriers.

Chapter 6

Summary

The key contributions of the thesis are:

- A new method to design turbo block code base on the realization of Golay sequences as cosets of the first order Reed-Muller codes was proposed. This method was shown to have significant power gain compared to the conventional turbo codes. The rate of this method may be low for some application. We thus have proposed a method to improve up on the code rate by utilization of QPSK modulation and multiple cosets of Reed-Muller codes.

- A new code based on dual BCH code was proposed that is amenable to a simple MAP decoding algorithm. It was shown that the TBC structure with the new code as a frequency component code and BCH as a time component code provide significant power gain over turbo code.

- We proposed a PAPR reduction method that can be applied for any channel coding scheme amenable to MAP decoding. This method shifts the PAPR ccdf

of original system to the left without any significant performance loss. We applied this method to a capacity achieving code, namely turbo code and have shown performance close to Shannon limit with significant low PAPRs.

Appendix A

Decoding Algorithms

A.1 MAP algorithm for Reed-Muller code

The algorithm was directly taken from [24].

Let us consider the transmission of a binary phase-shift keying (BPSK) modulated binary code over an additive white Gaussian channel. The two conditional pdf's of the received symbol y are given by

$$f_0(y) = \Pr(y \mid 0) = \frac{1}{\sqrt{2\pi}\sigma} e^{\frac{(y-1)^2}{2\sigma^2}},$$
$$f_1(y) = \Pr(y \mid 1) = \frac{1}{\sqrt{2\pi}\sigma} e^{\frac{(y+1)^2}{2\sigma^2}}.$$

Since we assume a memoryless channel, the probability of receiving a real vector $\boldsymbol{y} = (y_0, y_1, \cdots, y_{n-1})$ conditioned on a binary vector $\boldsymbol{c} = (c_0, c_1, \cdots, c_{n-1})$ being transmitted can be written as the product

$$\Pr(\boldsymbol{y} \mid \boldsymbol{c}) = \prod_{j=1}^{n} \Pr(y_j \mid c_j) \tag{A.1}$$

The idea of MAP decoding of binary first-order Reed-Muller code is based on two fold use of fast Hadamard transform, which we denote by $\mathbf{FHT_R}$. First, we use this transform for fast computation of probabilities $\Pr(\boldsymbol{y} \mid c_j)$. Next, after some auxiliary computations, we use this transform for fast computation of soft decisions (LLR's) $\ln\Pr(c_j = 0 \mid \boldsymbol{y}) - \ln\Pr(c_j = 1 \mid \boldsymbol{y})$ for all transmitted bits. The algorithm starts with computation of the vector $\boldsymbol{b} = (b_0, b_1, \cdots, b_{n-1})$, where

$$b_j = \ln \Pr(y_j \mid 0) - \ln \Pr(y_j \mid 1), j = 0, 1, \cdots, n-1, \tag{A.2}$$

$$t_i = \sum_{j=1}^{n} \ln \Pr(y_j \mid c_{ij}) - \sum_{j=1}^{n} \ln \Pr(y_j \mid c_{ij} \oplus 1), i = 0, 1, \cdots, 2^k - 1, \tag{A.3}$$

where $\oplus$ denote the addition in $\mathbb{F}_2$. We can compute the vector $\boldsymbol{t}$ with the help of $\mathbf{FHT_R}$ transform as $\boldsymbol{t} = (t_0, t_1, \cdots, t_{2^m-1}) = \mathbf{FHT_R}(b_0, b_1, \cdots, b_{n-1})$.

We use the following simple method to compute the sums of logarithms of probabilities from the differences of the sums. Let

$$s = \sum_{j=1}^{n-1} \ln \Pr(y_j \mid 0) + \ln \Pr(y_j \mid 1) \tag{A.4}$$

Then

$$r_i^{(0)} = \frac{s + t_i}{2} = \sum_{j=0}^{n-1} \ln \Pr(y_j \mid c_{ij}), \tag{A.5}$$

and

$$r_i^{(1)} = \frac{s - t_i}{2} = \sum_{j=0}^{n-1} \ln \Pr(y_j \mid c_{ij} \oplus 1), \tag{A.6}$$

$$v_i^{(0)} = e^{r_i^{(0)}} = \prod_{j=0}^{n-1} \ln \Pr(y_j \mid c_{ij}) \tag{A.7}$$

and

$$v_i^{(1)} = e^{r_i^{(1)}} = \prod_{j=0}^{n-1} \ln \Pr(y_j \mid c_{ij} \oplus 1) = \Pr(\boldsymbol{y} \mid \boldsymbol{c}_i \oplus 1). \tag{A.8}$$

This finishes the first part of the algorithm. The second part of the algorithm is concerned with computing soft decisions $\ln\Pr(c_j = 0 \mid \boldsymbol{y}) - \ln\Pr(c_j = 1 \mid \boldsymbol{y})$ Let us notice that if C is an $[n, k+1]$ code that contains the all-one codeword and

$$x_i = \Pr(\boldsymbol{y} \mid \boldsymbol{c}_i) - \Pr(\boldsymbol{y} \mid \boldsymbol{c}_i \oplus 1), i = 0, 1, \cdots, s^k - 1 \tag{A.9}$$

then the entries of the vector $(w_0, w_1, \cdots, w_{n-1})$ are equal to

$$\begin{aligned} w_j &= \sum_{i=0}^{2^k-1} d_{ij}(\Pr(\boldsymbol{y} \mid \boldsymbol{c}_i) - \Pr(\boldsymbol{y} \mid \boldsymbol{c}_i \oplus 1)) \\ &= \sum_{\boldsymbol{c} \in C_j^{(0)}} \Pr(\boldsymbol{y} \mid \boldsymbol{c}) - \sum_{\boldsymbol{c} \in C_j^{(1)}} \Pr(\boldsymbol{y} \mid \boldsymbol{c}), \end{aligned} \tag{A.10}$$

where d_{ij} is an i'th row and j'th column element of Hadamard matrix H_{2^m}.

For this, we can use the $\mathbf{FHT_R}$ transform for these computations. First, we form a vector $\boldsymbol{x}$ with entries $x_i = v_i^{(0)} - v_i^{(1)}$, and next compute $(w_0, w_1, \cdots, w_{n-1}) = \mathbf{FHT_R}(x_0, x_1, \cdots, x_{n-1})$. Therefore

$$\begin{aligned} w_j &= \sum_{\boldsymbol{c} \in RM(1,m)_j^{(0)}} \Pr(\boldsymbol{y} \mid \boldsymbol{c}) - \sum_{\boldsymbol{c} \in RM(1,m)_j^{(1)}} \Pr(\boldsymbol{y} \mid \boldsymbol{c}) \\ &= 2^{m+1}\Pr(\boldsymbol{y})(\Pr(c_j = 0 \mid \boldsymbol{y}) - \Pr(c_j = 1 \mid \boldsymbol{y})). \end{aligned} \tag{A.11}$$

Here, the expression $\boldsymbol{c} \in RM(1,m)_j^{(0)}$ refers to all codewords $\boldsymbol{c}$ whose j'th element are 0, and the expression $\boldsymbol{c} \in RM(1,m)_j^{(1)}$ refers to all codewords $\boldsymbol{c}$ whose j'th element are 1. The constant factor $2^{m+1}\Pr(\boldsymbol{y})$ can be computed as follows.

$$\begin{aligned} q &= \sum_{i=1}^{2^m-1} (v_i^{(0)} + v_i^{(1)}) \\ &= \sum_{\boldsymbol{c} \in RM(1,m)_j^{(0)}} \Pr(\boldsymbol{y} \mid \boldsymbol{c}) + \sum_{\boldsymbol{c} \in RM(1,m)_j^{(1)}} \Pr(\boldsymbol{y} \mid \boldsymbol{c}) \\ &= 2^{m+1}\Pr(\boldsymbol{y})(\Pr(c_j = 0 \mid \boldsymbol{y}) + \Pr(c_j = 1 \mid \boldsymbol{y})) \\ &= 2^{m+1}\Pr(\boldsymbol{y}). \end{aligned} \tag{A.12}$$

Finally, we compute the soft decisions or log likelihood ratios for all code bits as follows.

$$z_j = \frac{w_j}{q} = \Pr(c_j = 0 \mid \boldsymbol{y}) - \Pr(c_j = 1 \mid \boldsymbol{y}) \tag{A.13}$$

$$\mathrm{LLR}_j = \ln\frac{\Pr(c_j = 0 \mid \boldsymbol{y})}{\Pr(c_j = 1 \mid \boldsymbol{y})} = \ln\frac{1 + z_j}{1 - zj}. \tag{A.14}$$

A.2 MAP algorithm for BCH code

The algorithm was directly taken from [22].

Let us consider the transmission of binary elements {0,1} coded by a linear block code $C(n, k, \delta)$ on a Gaussian channel using binary symbols {-1, +1}. We shall consider the following mapping of the symbols $0 \rightarrow +1$ and $1 \rightarrow -1$. The observation $\boldsymbol{r} = (r_0, \cdots, r_l, \cdots, r_{n-1})$ at the output of the Gaussian channel for a transmitted codeword $\boldsymbol{e} = (e_0, \cdots, e_l, \cdots, e_{n-1})$is given by

$$\boldsymbol{r} = \boldsymbol{e} + \boldsymbol{g} \tag{A.15}$$

where components of $\boldsymbol{g} = (g_0, \cdots, g_l, \cdots, g_{n-1})$ are additive white Gaussian noise (AWGN) samples of standard deviation σ. By using maximum likelihood decoding (MLD), one can show that the optimum decision $\boldsymbol{d} = (d_0, \cdots, d_l, \cdots, d_{n-1})$ corresponding to the transmitted codeword $\boldsymbol{e}$.

If we let the reliability of decision d_j is defined using the LLR of transmitted symbol e_j, which is given by

$$\Lambda(d_j) = \ln(\frac{\Pr\{e_j = +1 \mid \boldsymbol{r}\}}{\Pr\{e_j = -1 \mid \boldsymbol{r}\}}) \tag{A.16}$$

the nominator of Equation (A.16) can be written as

$$\Pr\{e_j = +1 \mid \boldsymbol{r}\} = \sum_{\boldsymbol{c}^i \in \boldsymbol{S}_j^{+1}} \Pr\{\boldsymbol{e} = \boldsymbol{c}^i \mid \boldsymbol{r}\} \tag{A.17}$$

where $\boldsymbol{S}_j^{+1}$is the set of codewords $\{\boldsymbol{c}^i\}$ such that $c_j^i = +1$. And the denominator of Equation (A.16) can be written as

$$\Pr\{e_j = -1 \mid \boldsymbol{r}\} = \sum_{\boldsymbol{c}^i \in \boldsymbol{S}_j^{-1}} \Pr\{\boldsymbol{e} = \boldsymbol{c}^i \mid \boldsymbol{r}\} \tag{A.18}$$

where $\boldsymbol{S}_j^{-1}$is the set of codewords $\{\boldsymbol{c}^i\}$ such that $c_j^i = -1$. By applying Bayes' rule to Equation (A.17) and Equation (A.18) and assuming that the different codewords are uniformly distributed, we obtain for LLR, $\Lambda(d_j)$ the following expression:

$$\Lambda(d_j) = \ln\left(\frac{\sum_{\boldsymbol{c}^i \in \boldsymbol{S}_j^{+1}} \Pr\{\boldsymbol{r} \mid \boldsymbol{e} = \boldsymbol{c}^i\}}{\sum_{\boldsymbol{c}^i \in \boldsymbol{S}_j^{-1}} \Pr\{\boldsymbol{r} \mid \boldsymbol{e} = \boldsymbol{c}^i\}}\right) \tag{A.19}$$

where

$$\Pr\{\boldsymbol{r} \mid \boldsymbol{e} = \boldsymbol{c}^i\} = \left(\frac{1}{\sqrt{2\pi}\sigma}\right)^n \exp\left(-\frac{\mid \boldsymbol{r} - \boldsymbol{c}^i \mid^2}{2\sigma^2}\right) \tag{A.20}$$

$$\mid \boldsymbol{r} - \boldsymbol{c}^i \mid^2 = \sum_{l=0}^{n-1} (r_l - c_l^i)^2. \tag{A.21}$$

Let $\boldsymbol{c}^{+1(j)}$ and $\boldsymbol{c}^{-1(j)}$ be the codewords respectively, in $\boldsymbol{S}_j^{+1}$ and $\boldsymbol{S}_j^{-1}$, at minimum Euclidean distance from R. By combining Equation (A.19) and Equation (A.20), we obtain the following relation:

$$\Lambda(d_j) = \frac{1}{2\sigma^2}\left(\mid \boldsymbol{r} - \boldsymbol{c}^{-1(j)} \mid^2 - \mid \boldsymbol{r} - \boldsymbol{c}^{+1(j)} \mid^2\right) + \ln\left(\frac{\sum_i A_i}{\sum_i B_i}\right) \tag{A.22}$$

where

$$A_i = \exp\left(\frac{\mid \boldsymbol{r} - \boldsymbol{c}^{+1(j)} \mid^2 - \mid \boldsymbol{r} - \boldsymbol{c}^i \mid^2}{2\sigma^2}\right) \leq 1, \text{ with } \boldsymbol{c}^i \in S_j^{+1} \tag{A.23}$$

and

$$B_i = \exp(\frac{\mid \boldsymbol{r} - \boldsymbol{c}^{-1(j)} \mid^2 - \mid \boldsymbol{r} - \boldsymbol{c}^i \mid^2}{2\sigma^2}) \leq 1, \text{ with } \boldsymbol{c}^i \in S_j^{-1} \tag{A.24}$$

For high SNR, that is, $\sigma \to 0, \sum_i A_i \approx \sum_i B_i \to 1$ and thus the second term in Equation (A.22)tends to zero. By neglecting the second term in Equation (A.22), we obtain an approximation for the LLR of decision d_j equal to

$$\Lambda(d_j) = \frac{1}{2\sigma^2}(\mid \boldsymbol{r} - \boldsymbol{c}^{-1(j)} \mid^2 - \mid \boldsymbol{r} - \boldsymbol{c}^{+1(j)} \mid^2) \tag{A.25}$$

Therefore, computing the reliability of decision d_j at the output of the soft-input decoder requires two codewords $\boldsymbol{c}^{+1(j)}$ and $\boldsymbol{c}^{-1(j)}$. One of this codewords is the optimum decision codeword by Maximum likelihood Decoding (MLD). The optimum decision $\boldsymbol{d} = (d_1, \cdots, d_l, \cdots, d_n)$ corresponding to the transmitted codeword $\boldsymbol{e}$ is given by

$$\boldsymbol{d} = \boldsymbol{c}^i \text{ if } \mid \boldsymbol{r} - \boldsymbol{c}^i \mid^2 \leq \mid \boldsymbol{r} - \boldsymbol{c}^l \mid^2 \ \ \forall l \in [0, 2^k - 1], \ l \neq i \tag{A.26}$$

where $\boldsymbol{c}^i$ is the ith codeword and $\mid \boldsymbol{r} - \boldsymbol{c}^i \mid^2 = \sum_{l=0}^{n-1}(r_l - c_l^i)^2$. Then using an exhaustive search for the optimum codeword D, the computation complexity increases exponentially with k and becomes prohibitive for block code with $k > 6$. In order to have tolerable complexity for MLD, it is proposed to use Chase algorithm. [30] In 1972, Chase proposed a suboptimum algorithm of low complexity for near-ML decoding of linear block codes. This algorithm is based on the following observation. At high SNR, ML codeword $\boldsymbol{d}$ is located in the sphere of radius $(\delta - 1)$ centered on $\boldsymbol{y} = (y_0, \cdots, y_l, \cdots, y_{n-1})$, where $y_l = 0.5(1 + sgn(r_l))$ and $y_l \in \{0, 1\}$ with a very high probability. Thus, we can limit the reviewed codewords in Equation (A.26) to those in the sphere of radius $(\delta - 1)$ centered on $\boldsymbol{y}$. To reduce the number of reviewed codewords, only the set of the most probable codewords within the sphere are selected

by using channel information $\boldsymbol{r}$. The procedure used to identify the set of the most probable codewords is the following.

Step 1: Determine the position of the $p = \lfloor \delta/2 \rfloor$ least reliable binary elements of $\boldsymbol{y}$ using $\boldsymbol{r}$. The reliability of the elements of $\boldsymbol{y}$ will be defined later on.

Step 2: Form test patterns $\boldsymbol{t}^q$ defined as all the n-dimensional binary vectors with a single "1" in the least reliable positions and "0" in the other positions, two "1"s in the least reliable positions and "0" in the other positions, and $\cdots$, p "1"s in the least reliable positions and "0" in the other positions.

Step 3: Form test sequences $\boldsymbol{z}^q$ where $z_l^q = y_l \oplus t_l^q$ and decode $\boldsymbol{z}^q$ using an algebraic decoder and add the codeword $\boldsymbol{c}^q$ to subset $\boldsymbol{\Omega}$.

Decision D is then given by applying decision rule as given in Equation (A.26) with the reviewed codewords restricted to the subset of codewords Ω found at *step 3* above. Note that the components of the codewords are mapped from $0, 1$ to $+1, -1$ before computing the Euclidean distance. In *step 1*, the reliability of component y_j is defined using the log-likelihood ratio (LLR) of decision y_j

$$\Lambda(y_j) = \ln\left(\frac{\Pr\{e_j = +1 \mid r_j\}}{\Pr\{e_j = -1 \mid r_j\}}\right) = \left(\frac{2}{\sigma^2}\right) r_j \tag{A.27}$$

If we consider a stationary channel, we can normalize the LLR with respect to constant $2/\sigma^2$, and the relative reliability of y_j is then given by $\mid r_j \mid$.

Coming back to Equation (A.19), it is obvious that optimum decision $\boldsymbol{d}$ must be one of two codewords, $\boldsymbol{c}^{+1(j)}$ and $\boldsymbol{c}^{-1(j)}$. And we find the other one, which we shall call $\boldsymbol{c}$. C can be viewed as a competing codeword of D at minimum Euclidean distance

from R with $c_j \neq d_j$. Given codeword $\boldsymbol{d}$ and $\boldsymbol{c}$, we can show that the soft output given by Equation (A.25) can be expressed as the following equation:

$$\Lambda(d_j) = (\frac{|\,\boldsymbol{r}-\boldsymbol{c}\,|^2 - |\,\boldsymbol{r}-\boldsymbol{d}\,|^2}{2\sigma^2})d_j. \tag{A.28}$$

To find codeword $\boldsymbol{c}$, one must increase the size of the space scanned by the Chase algorithm. For that purpose, we increase the number of least reliable bits p used in the Chase decoder and also the number of test patterns. It is clear that the probability of finding $\boldsymbol{c}$ increases with the value of p. On the other hand, the complexity of the decoder increases exponentially with p and we must find a tradeoff between complexity and performance. This implies that in some cases we shall not be able to find a competing codeword $\boldsymbol{c}$. In the event where codeword $\boldsymbol{c}$ is not found, we must find another method for computing the soft output. One possible solution is to replace Equation (A.28)

$$\Lambda(d_j) = \beta \times d_j, \tag{A.29}$$

where β is given in [22], where it was optimized by trial and error.

Bibliography

[1] E. Dahlman, S. Parkvall, J. Skold, , and P. Beming. *Evolution: HSPA and LTE for Mobile Broadband*. Academic Press.

[2] D. Falconer, S.L. Ariyavisitakul, A. Benyamin-Seeyar, and B. Eidson. Frequency domain equalization for single-carrier broadband wireless systems. *Communications Magazine, IEEE*, 40(4):58 –66, apr 2002.

[3] S.H. Muller and J.B. Huber. A novel peak power reduction scheme for ofdm. In *Personal, Indoor and Mobile Radio Communications, 1997. 'Waves of the Year 2000'. PIMRC '97., The 8th IEEE International Symposium on*, volume 3, pages 1090 –1094 vol.3, sep 1997.

[4] S.H. Muller and J.B. Huber. A comparison of peak power reduction schemes for ofdm. In *Global Telecommunications Conference, 1997. GLOBECOM '97., IEEE*, volume 1, pages 1 –5 vol.1, nov 1997.

[5] Xiaodong Li and L.J. Jr. Cimini. Effects of clipping and filtering on the performance of ofdm. In *Vehicular Technology Conference, 1997, IEEE 47th*, volume 3, pages 1634 –1638 vol.3, may 1997.

[6] A.E. Jones, T.A. Wilkinson, and S.K. Barton. Block coding scheme for reduction of peak to mean envelope power ratio of multicarrier transmission schemes. *Electronics Letters*, 30(25):2098 –2099, dec 1994.

[7] A.E. Jones and T.A. Wilkinson. Combined coding for error control and increased robustness to system nonlinearities in ofdm. In *Vehicular Technology Conference, 1996. 'Mobile Technology for the Human Race'., IEEE 46th*, volume 2, pages 904 –908 vol.2, apr-1 may 1996.

[8] R.D.J. van Nee. Ofdm codes for peak-to-average power reduction and error correction. In *Global Telecommunications Conference, 1996. GLOBECOM '96. 'Communications: The Key to Global Prosperity*, volume 1, pages 740 –744 vol.1, nov 1996.

[9] H. Ochiai and H. Imai. Block coding scheme based on complementary sequences for multicarrier signals. volume E80-A, pages 2136–2143 vol.1, nov 1997.

[10] Jr. Cimini, L. Analysis and simulation of a digital mobile channel using orthogonal frequency division multiplexing. *Communications, IEEE Transactions on*, 33(7):665 – 675, jul 1985.

[11] T.A. Wilkinson and A.E. Jones. Minimisation of the peak to mean envelope power ratio of multicarrier transmission schemes by block coding. In *Vehicular Technology Conference, 1995 IEEE 45th*, volume 2, pages 825 –829 vol.2, jul 1995.

[12] K.G. Paterson and V. Tarokh. On the existence and construction of good codes with low peak-to-average power ratios. *Information Theory, IEEE Transactions on*, 46(6):1974 –1987, sep 2000.

[13] V. Tarokh and H. Jafarkhani. On the computation and reduction of the peak-to-average power ratio in multicarrier communications. *Communications, IEEE Transactions on*, 48(1):37 –44, jan 2000.

[14] J.A. Davis and J. Jedwab. Peak-to-mean power control in ofdm, golay complementary sequences, and reed-muller codes. *Information Theory, IEEE Transactions on*, 45(7):2397 –2417, nov 1999.

[15] C. Berrou, A. Glavieux, and P. Thitimajshima. Near shannon limit error-correcting coding and decoding: Turbo-codes. 1. In *Communications, 1993. ICC 93. Geneva. Technical Program, Conference Record, IEEE International Conference on*, volume 2, pages 1064 –1070 vol.2, may 1993.

[16] R. G. Gallager. *Low Density Parity Check Codes, Monograph*. M.I.T. Press.

[17] M. T. E. Golay. Multi-slit spectrometry. *J. Opt. Soc. Am.*, 39(6):437–437, Jun 1949.

[18] M. T. E. Golay. Static multislit spectrometry and its application to the panoramic display of infrared spectra. *J. Opt. Soc. Am.*, 41(7):468–472, Jul 1951.

[19] B.M. Popovic. Synthesis of power efficient multitone signals with flat amplitude spectrum. *Communications, IEEE Transactions on*, 39(7):1031 –1033, jul 1991.

[20] F.J. MacWilliams and N.J.A. Sloane. *The Theory of Error-Correcting Codes*. North-Holland.

[21] J. Hagenauer, E. Offer, and L. Papke. Iterative decoding of binary block and convolutional codes. *Information Theory, IEEE Transactions on*, 42(2):429 –445, mar 1996.

[22] R.M. Pyndiah. Near-optimum decoding of product codes: block turbo codes. *Communications, IEEE Transactions on*, 46(8):1003 –1010, aug 1998.

[23] J.A. Davis and J. Jedwab. Peak-to-mean power control and error correction for ofdm transmission using golay sequences and reed-muller codes. *Electronics Letters*, 33(4):267 –268, feb 1997.

[24] A. Ashikhmin and S. Litsyn. Simple map decoding of first-order reed-muller and hamming codes. *Information Theory, IEEE Transactions on*, 50(8):1812 – 1818, aug. 2004.

[25] Jr. Hammons, A.R., P.V. Kumar, A.R. Calderbank, N.J.A. Sloane, and P. Sole. The z4-linearity of kerdock, preparata, goethals, and related codes. *Information Theory, IEEE Transactions on*, 40(2):301 –319, mar 1994.

[26] Physical layer standard for cdma2000 spread spectrum systems.

[27] L. Bahl, J. Cocke, F. Jelinek, and J. Raviv. Optimal decoding of linear codes for minimizing symbol error rate (corresp.). *Information Theory, IEEE Transactions on*, 20(2):284 – 287, mar 1974.

[28] S. Lin and Jr. D.J. Costello. *Error Control Coding*. Prentice Hall.

[29] M. Sabbaghian and D.D. Falconer. An analytical approach for finite block length performance analysis of turbo frequency-domain equalization. *Vehicular Technology, IEEE Transactions on*, 58(3):1292 –1301, march 2009.

[30] D. Chase. Class of algorithms for decoding block codes with channel measurement information. *Information Theory, IEEE Transactions on*, 18(1):170 – 182, jan 1972.